The β-glucanase ZgLamA from Zobellia galactanivorans evolved a bent active site adapted for efficient degradation of algal laminarin.

Aurore Labourel, Murielle Jam, Alexandra Jeudy, Jan-Hendrik Hehemann, Mirjam Czjzek, Gurvan Michel

The β-glucanase *Zg*LamA from *Zobellia galactanivorans* evolved a bent active site adapted for efficient degradation of algal laminarin

Aurore Labourel[1,2], Murielle Jam[1,2], Alexandra Jeudy[1,2], Jan-Hendrik Hehemann[1,2§], Mirjam Czjzek[1,2] and Gurvan Michel[1,2*]

[1]UPMC University Paris 6, UMR 7139 Marine Plants and Biomolecules, Station Biologique de Roscoff, F-29682 Roscoff, Bretagne, France
[2]CNRS, UMR 7139 Marine Plants and Biomolecules, Station Biologique de Roscoff, F-29682 Roscoff, Bretagne, France

Running title: Complex structures of *Zg*LamA from *Zobellia galactanivorans*

[*]To whom correspondence should be addressed: Gurvan Michel, Station Biologique de Roscoff, Place Georges Teissier, 29680, Roscoff, Brittany, France ; Tel (33) 298 29 23 30; Fax (33) 298 29 23 24 ; E-mail: **gurvan@sb-roscoff.fr**
[§]current address: Department of Civil and Environmental Engineering, Massachusetts Institute of Technology, Cambridge, MA 02139, USA.

Keywords: laminarinase, 1,3 beta glucan, family GH16, marine bacteria, algae, crystal structure, glycoside hydrolase, oligosaccharide, carbohydrate metabolism

Background: The marine bacterium *Zobellia galactanivorans* consumes laminarin, a main algal storage polysaccharide, as carbon source.
Results: The β-glucanase *Zg*LamA$_{GH16}$ was structurally and biochemically characterized.
Conclusion: *Zg*LamA$_{GH16}$ evolved a unique bent active site making the enzyme highly efficient for laminarin degradation.
Significance: Within family GH16, highly specific laminarinase evolved from ancestral β-glucanases with a broader specificity.

ABSTRACT

Laminarinase is commonly used to describe β-1,3-glucanases widespread throughout Archaea, bacteria and several eukaryotic lineages. Some β-1,3-glucanases have already been structurally and biochemically characterized, but very few from organisms that are in contact with genuine laminarin, the storage polysaccharide of brown algae. Here we report the heterologous expression and subsequent biochemical and structural characterization of *Zg*LamA$_{GH16}$ from *Zobellia galactanivorans*, the first GH16 laminarinase from a marine bacterium associated with seaweeds. *Zg*LamA$_{GH16}$ contains a unique additional loop, compared to other GH16 laminarinases, which is composed of 17 amino-acids and gives a bent shape to the active-site cleft of the enzyme. This particular topology is perfectly adapted to the U-shape conformation of laminarin chains in solution, and thus explains the predominant specificity of *Zg*LamA$_{GH16}$ for this substrate. The 3D structure of the enzyme and two enzyme-substrate complexes, one with laminaritetraose, the other with a trisaccharide of 1,3-1,4-β-D-glucan, have been determined at 1.5 Å, 1.35 Å and 1.13 Å resolution, respectively. The structural comparison of substrate recognition pattern between these complexes allow the proposition that *Zg*LamA$_{GH16}$ likely diverged from an ancestral broad specificity GH16 β-glucanase and evolved toward a bent active site topology adapted to efficient degradation of algal laminarin.

INTRODUCTION

1,3-β-glucans constitute one of the main types of storage compounds in Eukaryotes (1). Their

biosynthesis is a very ancient pathway and likely coexisted with the glycogen metabolism in the last common ancestor of Eukaryotes (2). Storage 1,3-β-glucans are particularly well distributed in marine algae and these algal polysaccharides are structurally diverse. Euglenoid microalgae (Excavata phylum) store carbon as paramylon, a linear 1,3-β-glucan which is deposited as semi-crystalline granules in their cytosol (3). The storage polysaccharides of haptophyte phytoplanktons consist of β-1,3 and β-1,6-linked glucose polymers, but they are mainly composed of β-1,3 linkages in *Phaeocystales* (4), while the ratio β-1,6 / β-1,3 linkages is about 1.5 in *Coccolithales* (5). Soluble 1,3-β-glucans with occasional β-1,6-linked branches are the hallmark storage compounds of the Stramenopile phylum which includes diatoms (phytoplanktons), the multicellular brown algae and the non-photosynthetic phytopathogens Oomycetes. Diatoms and Oomycetes produce 1,3-1,6-β-glucans only constituted by glucose moieties, which are referred to as chrysolaminarin (6) and mycolaminarin (7), respectively. The storage polysaccharide of brown algae called laminarin, in reference to the *Laminaria* genus (kelp), has a slightly different structure. Like chrysolaminarin and mycolaminarin it is a small vacuolar polymer which contains on average 25 glucosyl residues and some occasional β-1,6-linked branches (8). But laminarin has the particularity to be composed of two series, the minor G-series which only contains glucose residues and the more abundant M-series which displays a D-mannitol residue at the reducing end (9). The unique presence of mannitol in laminarin is explained by a horizontal gene transfer event between the common ancestor of brown algae and an ancestral actinobacterium. This HGT event, which occurred after the divergence from Oomycetes and diatoms, had a major impact on the evolution of brown algae, resulting in the acquisition of the mannitol metabolism (2) and the biosynthetic route for alginate, the main cell wall polysaccharide of extant brown seaweeds (10).

Brown seaweeds and 1,3-β-glucan-producing microalgae represent a huge biomass in marine ecosystems. Brown algae dominate the intertidal and the upper sublittoral zones of rocky shores in temperate and polar regions and represent, with other marine macrophytes, a global carbon sink (11,12). Annually recurring phytoplankton blooms are large enough to be observed from space by satellites (13) and diatoms and haptophytes are frequently the dominant microalgal groups in such blooms (14,15). Therefore 1,3-β-glucans are abundant nutrients in marine trophic networks, and particularly, they constitute a crucial carbon source for specific marine heterotrophic bacteria (16,17). Moreover, a recent study of bacterioplankton responding to a spring diatom bloom in the North Sea has revealed a dynamic succession of distinct bacterial populations specialized for successive decomposition of algal biomass. The first bacterial peak, which was dominated by *Flavobacteria*, has been accompanied by a high abundance of family GH16 laminarinases (18), underlying the environmental importance of this class of glycoside hydrolases. *Flavobacteria* are also found associated to macroalgae and some species are specialists in the degradation of high molecular weight organic matter (19). This is the case of *Zobellia galactanivorans* which is a model microorganism for the bioconversion of algal polysaccharides. This marine flavobacterium isolated from the red alga *Delesseria sanguinea* in Roscoff (20) has been extensively studied for its capacity to degrade agars (21-23) and carrageenans (24,25) which are sulfated galactans from red algae. However, *Z. galactanivorans* is also able to metabolize some polysaccharides from brown algae, such as alginate. Indeed, this microorganism possesses two alginolytic operons induced by the presence of alginate (26) and the two first alginate lyases of this complex system (AlyA1 and AlyA5) have been recently characterized at the biochemical and structural level (27). *Z. galactanivorans* grows with brown algal laminarin as its sole carbon source and its genome contains five putative laminarinases: four of the family GH16 and one of the family GH64. This enzymatic diversity may seem surprising at first sight considering that laminarin is a small, soluble polysaccharide. It is difficult to predict whether these enzymes have redundant or complementary activities, or whether they match the biological diversity of 1,3-β-glucans present in the sea. Moreover, some laminarinases are also known to

be active on 1,3-1,4-β-glucans, adding another degree of complexity to the characterization of this group of enzymes. As a first step to an in depth understanding of the laminarin utilization system of *Z. galactinovorans,* we report here the biochemical and structural analysis of its first GH16 laminarinase, *Zg*LamA.

MATERIALS & METHODS

Except when mentioned, all chemicals were purchased from Sigma (France).

Cloning and site-directed mutagenesis of $ZgLamA_{GH16}$

The gene encoding the putative laminarinase *Zg*LamA (locus identifier: Zobellia_2431, Genbank accession number: CAZ96583) was cloned as in *Groisillier et al* (28). Briefly primers were designed to amplify the coding region corresponding to the catalytic module of LamA (forward primer gggggg**ggatcc**gcctttaataccttagtgttttcaga, reverse primer cccccc**caattg**ttattgatagatccttacatagtctatttc) by PCR from *Z. galactanivorans* genomic DNA. After digestion with the restriction enzymes BamHI and MfeI, the purified PCR product was ligated using the T4 DNA ligase into the expression vector pFO4 predigested by BamHI and EcoRI, resulting in a recombinant protein with a N-terminal hexa-histidine tag (plasmid $pLamA_{cat}$). The plasmid was transformed into *Escherichia coli* DH5α strain for storage and in *E. coli* BL21*(DE3)* strain for protein expression. Site-directed mutagenesis was performed using the Quick change II site-directed mutagenesis kit (Stratagene) and the previous plasmid. The two putative catalytic residues E269 and E274 were replaced either by a serine or an alanine (mutant E269A: forward primer tggcccgcatgcggc**gca**attgacattctggaa, reverse primer ttccagaatgtcaat**tgc**gccgcatgcgggcca; mutant E269S: forward primer tggcccgcatgcggc**tca**attgacattctggaa, reverse primer ttccagaatgtcaat**tga**gccgcatgcgggcca; mutant E274A: forward primer gaaattgacattctg**gca**caaaacggctgggac, reverse primer gtcccagccgttttg**tgc**cagaatgtcaatttc; mutant E274S: forward primer gaaattgacattctg**tca**caaaacggctgggac, reverse primer gtcccagccgttttg**tga**cagaatgtcaatttc). Mutant plasmids were sequenced to confirm that the mutation occurred at the correct position. These variant plasmids were also transformed into *E. coli* DH5α strain for storage and in *E. coli* BL21(*DE3*) strains for protein expression.

Overexpression and purification of $ZgLamA_{GH16}$ and $ZgLamA_{GH16\text{-}E269S}$.

E. coli BL21(*DE3*) cells harboring the plasmid $pLamA_{cat}$ were cultivated at 20°C in a 1 L auto-induction ZYP 5052 medium (29) supplemented with 100 $\mu g.mL^{-1}$ ampicillin. Cultures were stopped when the cell growth reached the stationary phase and were centrifuged for 35 min at 4°C, 3000 *g*. The cells were resuspended in a 20 mL of buffer A (50 mM HEPES, pH 7.5, 500 mM NaCl, 50 mM imidazole). An anti-proteases mixture (Complete EDTA-free, Roche™) and 0.1 mg / mL of DNase were added. The cells were disrupted in a French press. After centrifugation at 12500 *g* for 2 h at 4°C the supernatant was loaded onto a 10 mL Sepharose column (GE Healthcare) previously charged with $NiSO_4$ 100 mM and equilibrated with buffer A. The column was washed with buffer A (90 mL) and the protein was eluted with 60 mL of linear gradient between buffer A and buffer B (50 mM HEPES, pH 7.5, 500 mM NaCl, 500 mM imidazole) with a flow rate at 1 $mL.min^{-1}$. The different fractions (1 mL each) were analyzed by sodium dodecyl sulfate-polyacrylamide gel electrophoresis (SDS-PAGE). The fractions corresponding to a single band at the expected size (28 kDa) were pooled (47 mL) and were concentrated by ultrafiltration on an Amicon membrane (10 kDa-cutoff) (30 mL at 9 $mg.mL^{-1}$). An aliquot of 5 mL (9 $mg.mL^{-1}$) was loaded onto a 120 ml Superdex 75 (GE Healthcare) column previously equilibrated with buffer C (20 mM tris pH7.5, 200 mM NaCl). The protein was eluted using between 70 and 80 ml of buffer C and the purity of the fractions was checked by SDS-PAGE. A calibration curve was also used to determine the oligomerization state of $ZgLamA_{GH16}$. The mutant protein $ZgLamA_{GH16\text{-}E269S}$ was produced by the same procedure and was purified by a single step of metal affinity chromatography as describe above. The buffer A was composed of 20 mM tris pH7.5, 300 mM NaCl and 10 mM imidazole. The protein was eluted with a linear gradient of imidazole (10 mM to 600 mM) with a flow rate at 1 $mL.min^{-1}$. $ZgLamA_{GH16\text{-}E269S}$ was dialyzed (MWCO 6-8000

Spectrum Laboratories) to eliminate imidazole. Finally, *Zg*LamA$_{GH16}$ and *Zg*LamA$_{GH16\text{-}E269S}$ were concentrated by ultrafiltration on an Amicon membrane (10 kDa-cutoff) to 10 mg.mL^{-1} and 14.6 mg.mL^{-1} respectively. In addition, the proteins were filtrated on an Ultra free Durapore PVDF 0.1 µm membrane before crystallization screening.

Thermostability analysis.
The thermostability of *Zg*LamA$_{GH16}$ was studied by dynamic light scattering (DLS). A solution of 50 µL of *Zg*LamA$_{GH16}$ at 10 mg.mL^{-1} was filtered on a 0.2 µm membrane. Using a Zetasizer Nano instrument (Malvern), the protein solution was heated from 10°C to 70°C in steps of 1°C during a total period of 12 h and the hydrodynamic gyration radius (Rg) was measured at each degree. The denaturation temperature was determined as the point of sharp change in gyration radius.

Enzymatic activity assays on β-glucans
The hydrolytic activities of the purified *Zg*LamA$_{GH16}$ and *Zg*LamA$_{GH16\text{-}E269S}$ were measured by the ferricyanide reducing sugar assay (30) on different β-glucans: laminarin from *Laminaria digitata* (0.1% w/v), mixed-linked glucan (MLG) from *Barley*, curdlan from *Alcaligenes faecalis* and paramylon from *Euglena gracilis* (all at 0.2% w/v). Laminarin is a small polysaccharide and has a large amount of reducing ends, thus this substrate was reduced prior to use. 70 mg of $NaBH_4$ were added to 10 mL of laminarin (20 mg.mL^{-1}) and the mixture was incubated at 20°C for three days. The solution was acidified by adding concentrated acetic acid, drop by drop, until H_2 release stopped. 40 mL of absolute ethanol were added, and after centrifugation the pellet was resuspended in 50 mL absolute ethanol. This washing step was repeated twice, and the pellet was finally dried in vacuum (SpeedVac).
Reduced laminarin was hydrolyzed by 0.7 µM of purified enzyme in a 1 mL of buffer C at 40°C for 30 min. Aliquots of the reaction mixture (40 µL) were taken at T_0, 10 min and 30 min and added to 200 µL of 5X ferricyanide reagent. The samples were boiled at 95°C for 15 min and cooled to 20°C before absorbance measurement at 420 nm. All experiments were undertaken in triplicate. A calibration curve with 0-3.33 mM (0; 0.278; 0.556; 1.11; 1.67; 2.22; 2.78; 3.33) glucose was used to calculate the amount of released reducing ends as glucose-reducing-end equivalents. The activity of *Zg*LamA$_{GH16}$ on MLG, curdlan and paramylon was measured similarly, except that the reactions were monitored for 15 h. Aliquots were taken at T_0, 10 min, 1 h, and 15 h.
The pH optimum for laminarin hydrolysis was determined as follows; 0.06% (w/v) of laminarin were hydrolyzed by 10 nM of *Zg*LamA$_{GH16}$ in a 1 mL reaction mixture at 40°C for 10 min. The following different buffers (at 100 mM) were tested with the pH varying from 4 to 9 by 0.5 increments of pH unit: phosphate citrate (pH 4 to 6), 2-morpholinoethanesulfonic-acid-NaOH (MOPS, pH 6 to 7.5), tris-HCl (pH 7.5 to 8.5), glycine-NaOH (pH 8.5 to 9). Released reducing ends were measured as described above, except that aliquots of reaction mixture (40 µL) were taken every 2 min.
The kinetic parameters of *Zg*LamA$_{GH16}$ on reduced laminarin and MLG were determined using 10 nM of enzyme in a reaction mixture of 500 µL at optimal temperature and pH. The amount of released reducing ends was measured as above. For each substrate, five concentrations were used: 0.06% (w/v), 0.12%, 0.24%, 0.48%, and 0.96% for laminarin; 0.05% (w/v), 0.1%, 0.15%, 0.2% and 0.25% for MLG. Aliquots of the reaction mixture (40 µL) were taken every 2 min for 10 min for laminarin and every 15 min for 1 h for MLG. For each substrate, the *K*m and k_{cat} were determined from a Lineweaver-Burk plot.

Fluorophore Assisted Carbohydrate Electrophoresis (FACE) analysis.
0.5% (w/v) of laminarin was hydrolyzed using 100 nM of *Zg*LamA$_{GH16}$ in a reaction mixture of 500 µL of glycine buffer pH 8.5 at 20°C. An aliquot of 20 µL (100 µg of oligosaccharides) was taken at 30 second, 1 min, 2 min, 5 min, 15 min, 30 min and 1 h. The samples were boiled to inactivate the enzyme and then dried in vacuum (SpeedVac). The FACE experiment was undertaken as previously described (31). Briefly, the oligosaccharides were mixed to 2 µL of ANTS 0.15 M and 5 µL of $NaBH_3CN$ 1M. The reaction mixtures were incubated at 37°C for at

least 3 h and dried in vacuum (SpeedVac). The oligosaccharides were resuspended in 20 µL of glycerol 25% and 10 µL (50 µg) were loaded into a 36% acrylamide gel. The migration was undertaken at 200V, 4°C and with a 1X migration buffer (192 mM glycine, 25 mM Tris, pH8.5). The experiment was repeated using 0.5% (w/v) of MLG and 4.5 µM of $ZgLamA_{GH16}$. The reaction mixture was incubated at 40°C and an aliquot of 20 µL was taken at 2 min, 5 min, 15 min and 30 min.

100 µg of different commercial linear 1,3-β-D-glucans (Megazyme) (trisaccharide, tetrasaccharide, pentasaccharide and hexasaccharide) were hydrolyzed using 4.5 µM of $ZgLamA_{GH16}$ in a reaction mixture of 100 µL of glycine buffer pH 8.5 at 40°C for 12 h. For each sample, an aliquot containing 50 µg of oligosaccharides were treated as mentioned above. 5 µL (12.5 µg) were loaded into a 36% acrylamide gel.

A glucan tetrasaccharide containing two β-1,4 linkages separated by one β-1,3 linkage (G4G3G4G) was also purchased from Megazyme. Three samples of this substrate at 50 µg were labeled with ANTS as previously described. One of them was used as control. The second sample was resuspended in a reaction mixture of 50 µL containing 4.5 µM of $ZgLamA_{GH16}$ and glycine buffer pH8.5 at 37°C for 30 min. The same experiment was undertaken on the third sample except that $ZgLamA_{GH16}$ was first inactivated by heating. In parallel, 100 µg of non-labeled G4G3G4G was hydrolyzed by $ZgLamA_{GH16}$ at 37°C for 30 min. After the enzymatic reaction, an aliquot containing 50 µg of oligosaccharides (reaction products) was labeled as mentioned above. A sample of 50 µg of glucose was also labeled with ANTS and was used as control. 10 µL (25 µg) of each samples were loaded onto a 36% acrylamide gel.

Crystallization of $ZgLamA_{cat}$ *and* $ZgLamA_{GH16\text{-}E269S}$*, structure determination and refinement.*

Crystallization screening was undertaken with the nanodrop-robot Honeybee (Cartesian) using the commercial screens PACT and JCSG+ (Qiagen). The initial crystallization conditions of $ZgLamA_{GH16}$ were manually optimized and single crystals were obtained as follows: 2 µL of enzyme at 10 $mg.mL^{-1}$ were mixed with 2 µL of reservoir solution containing 24% PEG 3350 and 100 mM Na citrate pH 5.2 in hanging drops at 4°C. Single crystals of $ZgLamA_{GH16\text{-}E269S}$ in complex with laminarin oligosaccharides were obtained from 2 µL of the mixture enzyme/oligosaccharides (13.3 $mg.mL^{-1}$ of enzyme, 5 mM of purified hexasaccharides) that were added to 1 µL of reservoir solution containing 100 mM MIB buffer pH 4.0 (sodium malonate, imidazole and boric acid) and 19% of PEG 1500 in hanging drops at 20°C. Single crystals of $ZgLamA_{GH16\text{-}E269S}$ in complex with MLG trisaccharides were obtained from 2 µL of the mixture enzyme/oligosaccharides (11.7 $mg.mL^{-1}$ of enzyme, 0.04% (w/v) of MLG degradation products) that were added to 1 µL of reservoir solution containing 100 mM MIB buffer pH 4.0, 17% of PEG 1500 and 10% of glycerol in hanging drops at 12°C. Prior to flash-freezing in a nitrogen stream at 100 K, single crystals were quickly soaked in the same crystallization solution supplemented with 10%, 20% or 12% glycerol, respectively. Diffraction data for $ZgLamA_{GH16}$ were collected on the beamline ID23-1 (ESRF, Grenoble, France). The diffraction data for the two complexes, $ZgLamA_{GH16\text{-}E269S}$ - laminarin and $ZgLamA_{GH16\text{-}E269S}$ - mix-linked-glucan were collected on the beamline ID29 (ESRF). X-ray diffraction data were integrated using Mosflm (32) and scaled with Scala (33). The structure of $ZgLamA_{GH16}$ was determined by molecular replacement with MolRep (34) using the chain A of *Rm*LamR from *Rhodothermus marinus* (PDB code 3ILN, 35) as a starting model. The structure of $ZgLamA_{GH16}$ was manually built using COOT (36). For both complexes of $ZgLamA_{GH16\text{-}E269S}$, the structures were also determined by molecular replacement, but using the coordinates of the chain A of $ZgLamA_{GH16}$. For all the structures, the initial molecular replacement solutions were further refined with the program REFMAC5 (37), alternating with cycles of manual rebuilding using COOT. A subset of 5% randomly selected reflections was excluded from computational refinement to calculate the R_{free} factors throughout the refinement. The addition of the ligand sugar units for the complexed structures was performed manually using COOT. Water molecules were added automatically with

REFMAC-ARP/wARP and visually verified. The final refinement was carried out using REFMAC5 with TLS, anisotropic B factors, and NCS restraints and babinet scaling. Data collection and refinement parameters are presented in Table 1. The atomic coordinates and structure factors of *Zg*LamA$_{GH16}$, *Zg*LamA$_{GH16\text{-}E269S}$-laminarin and *Zg*LamA$_{GH16\text{-}E269S}$-MLG (codes: 4BQ1, 4BOW and 4BPZ, respectively) have been deposited in the Protein Data Bank (PDB), Research Collaboratory for Structural Bioinformatics, Rutgers University, New Brunswick, NJ (http://www.rcsb.org/).

Sequence analysis and structure comparison.
The family GH16 laminarinases with known 3D crystal structures were selected in the CAZY database (http://www.cazy.org/, 38) and their amino-acid sequences were recovered in the PDB. These sequences and the *Zg*LamA$_{GH16}$ sequence were aligned using MAFFT (39). The multiple sequence alignment was manually refined using Bioedit, based on the superimposition of the structures of the different laminarinases. The crystal structure of ZgLamA$_{GH16}$ was compared with those of the laminarinase *Pc*Lam16A from *Phanerochaete chrysosporium* (PDB: 2W39, 40) and of the lichenase from *Fibrobacter succinogenes* (PDB: 1ZM1, 41) using COOT and Pymol. For phylogenetic analysis, close homologues of *Zg*LamA$_{GH16}$ and *Rm*lamR were selected on the basis of a BlastP search on Genbank NR. The selected proteins were subjected to multiple sequence alignment using MAFFT (42), with the iterative refinement method and the scoring matrix Blosum62. These alignments were manually edited using Bioedit (© Tom Hall). The phylogenetic tree was derived from the refined alignment using the Maximum Likelihood method with the program MEGA 5 (43). The reliability of the trees was tested by bootstrap analysis using 100 resamplings of the dataset.

RESULTS

ZgLamA$_{GH16}$ is a β-glucanase highly specific for laminarin.
In the genome of *Z. galactanivorans*, the gene *zg2431* is predicted to produce a putative laminarinase referred to as *Zg*LamA. This protein is predicted to be anchored in the outer membrane due to the presence of a lipoprotein signal peptide and displays a modular architecture (Fig. 1A). In the N-terminal region, the signal peptide is followed by a Polycysitic Kidney Disease (PKD)-like module composed of 102 residues. Such β-sandwich domains are often involved in protein-protein interactions (44). The C-terminal region is composed of a catalytic module of glycoside hydrolase family 16 (GH16). Within the GH16 family, two conserved glutamates in the pattern EXDX(X)E play the role of the catalytic residues (45). In *Zg*LamA, the equivalent to the nucleophile is Glu269, while the general acid/base is Glu274 (Fig. 1B). In order to study the enzymatic properties of *Zg*LamA without potential interference from the PKD module and also to facilitate crystallization assays, we have decided to only clone the nucleotide sequence corresponding to the GH16 catalytic module into the vector pFO4. The recombinant protein, referred to as *Zg*LamA$_{GH16}$, was produced in soluble form in *Escherichia coli* BL21(*DE3*) strain with a yield of about 300 mg per liter of culture. A step of immobilized metal ion affinity chromatography followed by size exclusion chromatography (SEC) was necessary to purify *Zg*LamA$_{GH16}$ to electrophoretic homogeneity. The SEC analysis suggested that *Zg*LamA$_{GH16}$ is a monomer in solution, and this result was confirmed by Dynamic Light Scattering (DLS) experiments. The DLS was also used to study the protein thermostability. Above 40°C a sharp increase of the hydrodynamic radius of gyration (Rg) is observed, indicating the beginning of the denaturation of *Zg*LamA$_{GH16}$.
The enzymatic activity of the purified *Zg*LamA$_{GH16}$ was screened by the ferricyanide reducing sugar assay on two soluble β-glucans, laminarin from *L. digitata* and 1,3-1,4-β-D-glucan from barley (mixed-linked glucan, MLG), and two crystalline 1,3-β-glucans, curdlan from *Alcaligenes faecalis* and paramylon from *Euglena gracilis*. Significant activity was detected in the presence of laminarin and MLG, but not on the crystalline glucans. Prior to determining the kinetic parameters of *Zg*LamA$_{GH16}$, the effect of pH on the enzyme activity was determined using laminarin. The maximum of activity is obtained at pH 8.5 in 0.1

M glycine buffer (Fig. 2A). *Zg*LamA$_{GH16}$ displays no activity at pH 4.0 in 0.1 M Phosphate citrate buffer. The activity is detectable from pH 4.5 and increases with the pH until 7.0 (in 0.1 M MOPS), reaching 92% of the maximum activity. In contrast, the tris buffer clearly has an inhibitory effect. In 0.1 M tris-HCl pH 8.5, *Zg*LamA$_{GH16}$ only reaches 30% of the optimal activity detected in glycine buffer at the same pH. Altogether, the highest activity was obtained in glycine-NaOH pH 8.5 but the exact pH optimum remains uncertain. The kinetic parameters of *Zg*LamA$_{GH16}$ were then measured at 40°C and in glycine-NaOH pH 8.5 on reduced laminarin and MLG. The turnover of *Zg*LamA$_{GH16}$ on laminarin is much higher than on MLG (410 and 32 s^{-1}, respectively), while its *K*m values for both substrates is relatively similar (*K*m 5.0 mM (0.9 $mg.mL^{-1}$) and 8.7 mM (1.57 $mg.mL^{-1}$), respectively) (Fig. 2B). Taking into account these two parameters, *Zg*LamA$_{GH16}$ has a catalytic efficiency (k_{cat}/Km) 22-fold higher on laminarin than on MLG.

The nucleophile candidate Glu269 was successfully replaced by a serine, by site-directed mutagenesis. The mutant variant *Zg*LamA$_{GH16\text{-}E269S}$ was also produced in *E. coli* BL21(*DE3*) in a soluble form with high yield (110 mg / liter of culture) and purified by nickel affinity chromatography. *Zg*LamA$_{GH16\text{-}E269S}$ (10 nM) was assayed on laminarin and MLG with reducing sugar assay as for *Zg*LamA$_{GH16}$, but no enzymatic activity was detected even after 24h of incubation (data not shown), confirming the involvement of Glu269 in the catalytic machinery of *Zg*LamA.

Hydrolysis pattern of laminarin and MLG oligosaccharides by ZgLamA$_{GH16}$.

The hydrolysis of laminarin and MLG by *Zg*LamA$_{GH16}$ was monitored by FACE for 1 h and 30 min, respectively (Fig. 3A,B). For both substrates, oligosaccharides of relative high degree of polymerization were initially released, progressively followed by oligosaccharides of smaller sizes. These patterns of action indicate that *Zg*LamA$_{GH16}$ proceeds according to an endolytic mode of action. The degradation products of *Zg*LamA$_{GH16}$ were further analyzed by two different approaches. For laminarin, four standard β-1,3-glucan oligosaccharides purchased from Megazyme (DP range from 3 to 6) were digested by *Zg*LamA$_{GH16}$ to completion. The reducing ends of the reaction products were labeled with ANTS and analyzed by FACE (Fig. 3C). After the hydrolysis of the trisaccharide, a reaction product corresponding to a disaccharide is observed. The released monosaccharide is only partially visible, because it is almost masked by the migration front of the fluorescent marker. For the others oligosaccharides, the same degradation pattern is observed (Fig. 3C). This experiment indicates that the smallest oligosaccharide that can be degraded by *Zg*LamA$_{GH16}$ is laminaritriose and the terminal products are glucose and laminaribiose.

In order to determine which linkage in MLG is hydrolyzed by *Zg*LamA$_{GH16}$, a glucan tetrasaccharide containing two β-1,4 linkages separated by one β-1,3 linkage (G4G3G4G) was purchased from Megazyme. If the enzyme cleaved the β-1,3 linkage, two disaccharides G4G would be released, migrating as a single band. In the case of the cleavage of a β-1,4 linkage, a glucose and a trisaccharide G4G3G would be released. When the active *Zg*LamA$_{GH16}$ is added to the previously labeled oligosaccharide, no reaction product is observed compared to the controls (Fig. 3D), suggesting that the ANTS labeling precludes the action of *Zg*LamA$_{GH16}$. When the labeling is undertaken after the enzymatic reaction the reaction products migrate as two bands, corresponding to a monosaccharide and a trisaccharide (Fig. 3D). Therefore, these experiments indicate that *Zg*LamA$_{GH16}$ specifically cleaves β-1,4 linkages next to β-1,3 linkages. The trisaccharide G4G3G was not further degraded indicating that glucose and the MLG trisaccharide are the terminal products.

Crystal structure of ZgLamA$_{GH16}$.

The crystal structure of *Zg*LamA$_{GH16}$ was solved at a resolution of 1.5 Å by molecular replacement using the laminarinase *Rm*LamR from *Rhodothermus marinus* (35). The crystal is orthorhombic ($P2_12_12_1$) and its asymmetric unit contains two chains of *Zg*LamA$_{GH16}$, two glycerol molecules, two calcium ions (one of each in each protein monomer) and a total of 526 water molecules. Chains A and B are composed of 251 amino acids (from His133 to Gln383)

respectively. The overall structure of *Zg*LamA$_{GH16}$ confirms that this protein adopts the jelly roll fold typical of GH16 enzymes. The core enzyme is composed of 15 β-strands forming two twisted β-sheets. Some loops extend from the binding cleft in the regions connecting the two β-sheets. Particularly, *Zg*LamA$_{GH16}$ displays a long loop which is not present in other known structures of family GH16 laminarinases (Fig. 1). This additional loop is composed of 17 amino-acids (from Ala246 to Ala262) and appears to block the negative subsites (Fig. 4A) (subsite naming according to Davies and coworkers, 46) in comparison to the straight groove observed in *Rm*LamR (Fig. 4B). The entire loop can be perfectly superimposed between the *Zg*LamA$_{GH16}$ enzyme structure and that of its complexes (see below). Moreover, the B factors of the atoms composing this additional loop are not significantly different from the B factors of other protein atoms. Some strong hydrogen bonds are involved in the stability of the loop (distances are given for chain A). Glu250 $O^{\varepsilon 2}$ is stabilized by Gln160 $N^{\varepsilon 2}$ (2.80 Å), Arg213 $N^{\eta 2}$ (2.73 Å) and Tyr350 O^{η} via a structural water molecule (Glu250-HOH 2.74 Å and HOH-Tyr350 2.62 Å). The hydroxyl group of this tyrosine is also bound to Ser248 O^{γ} (2.96 Å). The carbonyl group of Gly252 is bound to His158 $N^{\varepsilon 2}$ (2.86 Å). Hydrophobic interactions are also involved in the stability of this loop conformation. Tyr254 is surrounded by Lys217, His158 and Phe255. Taking into account all these elements, this additional loop seems to be stable and provides a bend in the catalytic cleft (Fig. 4C). A calcium ion is found on the convex side of each protein chain and is bound to the carbonyl and carboxylate O atoms of Asp377, the carbonyl O atom of Gly189, the carboxylate O atoms of Glu147 and Glu145, as well as one water molecule in an octahedral geometry. With the exception of plant xyloglucan endotransglycosylases / hydrolases (47,48), such a calcium binding site is well conserved in the GH16 enzymes (49) and this cation is known to increase their thermostability (50). A glycerol molecule is bound to subsite -1 of the catalytic cleft of each *Zg*LamA$_{GH16}$ monomer mimicking a bound glucose moiety. The carbon backbone of the glycerol is stacked against the aromatic rings of Trp238 and Trp242; the hydroxyl group O3 is hydrogen-bonded to Trp238 $N^{\varepsilon 1}$ (3.11Å) and Glu274 $O^{\varepsilon 1}$ (2.82 Å), while the hydroxyl group O1 makes a strong hydrogen bond to Glu269 $O^{\varepsilon 2}$ (2.61 Å).

Structure of ZgLamA$_{GH16\text{-}E269S}$ complexes: molecular basis of laminarin and MLG recognition.

The inactive mutant *Zg*LamA$_{GH16\text{-}E269S}$ was co-crystallized with either purified laminarin hexasaccharides or MLG terminal degradation products, both types of oligosaccharides being produced by *Zg*LamA$_{GH16}$. The two complex structures were determined at a resolution of 1.35 Å and 1.13 Å respectively by molecular replacement using *Zg*LamA$_{GH16}$ as a model. The unit cells of these complex crystals and their symmetry was similar to that of the native crystal. In both complex structures, the conserved cation binding site on the convex side of the protein is occupied by a calcium ion, as observed in the structure of *Zg*LamA$_{GH16}$.

The asymmetric unit of the "laminarin complex" crystal contains two *Zg*LamA$_{GH16\text{-}E269S}$ molecules (from Ala136 to Gln383), a sodium ion, two calcium ions, and 545 water molecules. Each protein chain binds a laminarin oligosaccharide, but only 3 glucose units are visible in chain A (subsites -1 to -3) while four glucose moieties were modeled in chain B (subsites -1 to -4). In both cases, the missing units of the laminarihexaoses are localized in the solvent region without contact to the protein and thus likely disordered. Except in a few cases (23), an oligosaccharide spanning the negative and positive subsites is rarely observed in complexed structures of enzymes from Clan GH-B (GH7 and GH16). Indeed, the sugar in subsite -1 is expected to bind with a distorted skew boat conformation in order to give rise to the preferred axial orientation for the leaving group (51). Such a distorted conformation is unstable, explaining the usual difficulty to obtain a simultaneous occupation of negative and positive subsites in Clan GH-B enzymes. Due to the high resolution of the enzyme-complex structure determination we see alternate conformations for these oligosaccharides. In chain B, the D-glucose residue in subsite -1 displays both α and β conformation for the hydroxyl group of the anomeric carbon C1, confirming that the sugar at

subsite -1 is the reducing end of the oligosaccharide. Due to the replacement of the nucleophile Glu269 by a serine, the glucose in α conformation mimics the expected glycosyl-enzyme intermediate conformation. For both laminarin oligosaccharides, the electron density of the glucose residues in subsites -1, -2 and -3 are perfectly defined. The fourth glucose moiety is more disordered. In chain B, the four visible linked glucose units adopt a helical conformation, confirming the tendency of β-1,3-glucans to form helices (Fig. 4E). In both independent *Zg*LamA$_{GH16}$ chains the three first negative subsites are similar (Fig. 5A,B). In subsite -1, the glucose unit in the α configuration binds like the glycerol molecule in the native structure of *Zg*LamA$_{GH16}$ and forms similar hydrogen bonds with Glu274 and Trp238, as well as with three additional residues Asp271, Asn171 and Ser269. This glucose unit forms a hydrophobic interaction with Trp238 and Trp242, the latter being conserved in all family GH16 enzymes, in which it constitutes a hydrophobic platform correctly orienting the sugar ring at the -1 subsite (49). The subsite -2 is characterized by hydrogen bonds between the glucose unit and three polar amino-acids (Asn171, Glu250 and Arg213), Glu250 belonging to the additional loop unique to *Zg*LamA. As mentioned before, Arg213 plays an important role in the stability of this loop by forming a hydrogen bond with Glu250. Moreover, this arginine likely orients Glu250 to properly interact with the substrate. The glucose unit at subsite -2 is sandwiched by Trp264 and His170. The ~90° orientation between Trp242, situated below the sugar in subsite -1, and His 170 and Trp264 , which sandwhich the sugar in subsite -2, precisely orients the laminarin chain towards the catalytic center. Finally, the glucose in subsite -3 is stabilized by a hydrogen bond between its hydroxyl group Glc3 O6 with the carbonyl of Trp264, while the fourth glucose does not form any direct interactions with the protein. A structural water molecule, conserved in the two protein chains (HOH164 in chain A and HOH138 in chain B) also stabilizes the laminarin oligosaccharide by making indirect interactions with the enzyme.

The asymmetric unit of the "MLG complex" crystal contains two *Zg*LamA$_{GH16\text{-}E269S}$ molecules (from His133 to Gln383 for chain A, and from His132 to Gln383 for chain B), two calcium ions, and 585 water molecules. Three glucose units of a MLG oligosaccharide are clearly visible in the negative subsites of each enzyme. A β-1,3-linkage is observed between subsites -1 and -2, while a β-1,4-linkage is positioned between subsites -2 and -3 (Fig. 6A,B). Even when decreasing the sigma-level of the difference electron density map to 0.5 does not reveal any additional glucose moiety, indicating that the oligosaccharide bound to *Zg*LamA$_{GH16\text{-}E269S}$ is a trisaccharide, consistent to the result obtained with the FACE experiment (Fig. 3D). The glucose units in the subsites -1 and -2 bound similar to the laminarin oligosaccharide, except for the loss of the hydrogen bond between Glc2 O6 and Arg213 $N^{\eta 2}$ (Fig. 6A,B). In subsite -3, the presence of a β-1,4-linkage in the MLG trisaccharide produces a 180° rotation of the third glucose in comparison to the laminarin hexasaccharide, resulting in a totally different recognition of this moiety. The interaction of the hydroxyl group Glc3 O6 with the carbonyl group of Trp264, observed in the laminarin complex (Fig. 5A,B), is replaced by the formation of a hydrogen bond between the hydroxyl group Glc3 O3 and Glu263 $O^{\varepsilon 2}$ in the MLG complex (Figure 7B). A structural water molecule (HOH139 in chain A and HOH166 in chain B) is also involved in the stability of the MLG complex.

Comparison of ZgLamA$_{GH16\text{-}E269S}$ substrate complexes with other β-glucanase complexes.

The *Zg*LamA$_{GH16\text{-}E269S}$ complexes have been compared to other GH16 β-glucanases for which complex structures are available: the laminarinase *Pc*Lam16A from the terrestrial fungus *Phanerochaete chrysosporium* (PDB code 2W39, EC 3.2.1.6, 40) and the lichenase TFsβ-glucanase from the bovine rumen bacterium *Fibrobacter succinogenes* (PDB code 1ZM1, EC 3.2.1.76, 41). *Pc*Lam16A was initially co-crystallized with a MLG trisaccharide G4G3G, but only a G3G disaccharide spanning the subsites -1 and -2 was discernible in the electron density map (40). The subsites -1 of *Zg*LamA$_{GH16\text{-}E269S}$ and *Pc*Lam16A are well conserved. The tryptophan residues

Trp99 and Trp103 of *Pc*Lam16A are oriented in the same way as Trp238 and Trp242, respectively (Fig. 5C). *Pc*Lam16A displays an additional residue, Asn162, showing two conformers. The 'swung-in" conformer makes a hydrogen bond with the hydroxyl group O2 of the glucose residue bound to subsite -1. In subsite -2 two residues are also conserved, Arg70 and Trp110 in *Pc*Lam16A corresponding to Arg213 and Trp264 in *Zg*LamA$_{GH16-E269S}$. The conserved relative orientation of the tryptophan side-chains in subsites -1 and -2 is a critical feature explaining why both *Zg*LamA$_{GH16-E269S}$ and *Pc*Lam16A require a β-1,3-linkage between subsites -1 and -2. In *Zg*LamA$_{GH16-E269S}$ three additional residues strengthen the binding of the glucose moiety in subsite -2; these are: Glu250, which belongs to the loop unique to *Zg*LamA$_{GH16-E269S}$, His170 and Asn171. Subsite -3 of *Zg*LamA$_{GH16-E269S}$ is essentially constituted by Trp264, but this key tryptophan is not conserved in *Pc*Lam16A. Moreover, the third glucose of the trisaccharide co-crystallized with *Pc*Lam16A was disordered, suggesting that this GH16 enzyme does not possess a third negative subsite (Fig. 5C).

The lichenase TFsβ-glucanase is strictly specific for MLG and was co-crystallized with a MLG trisaccharide (G4G3G) (41). With the exception of the conserved catalytic residues, *Zg*LamA$_{GH16-E269S}$ and TFsβ-glucanase have very few features in common (Fig. 6C). Both have three negative subsites, but only the binding mode in subsite -1 is partially similar with the conservation of an aromatic residue (Trp242 in *Zg*LamA$_{GH16-E269S}$, Phe40 in TFsβ-glucanase) providing a hydrophobic platform for the inferior face of the glucose moiety. The conserved tryptophan Trp141 (Trp238 in *Zg*LamA$_{GH16-E269S}$) is hydrogen-bonded through its intracyclic 2-amino group to the glucose hydroxyl group O6. All other residues involved in MLG recognition are not conserved between *Zg*LamA$_{GH16-E269S}$ and TFsβ-glucanase. The orientation of the MLG trisaccharides are also completely different, parallel to the inner β-sheet in TFsβ-glucanase (Fig. 6C), while this oligosaccharide diverges from the *Zg*LamA$_{GH16-E269S}$ β-sheet by an angle of about 60° (Fig. 6B).

DISCUSSION

In its natural environment a marine bacterium such as *Zobellia galactanivorans* can feed on different types of 1,3-β-glucans, from soluble, branched laminarin from brown algae, diatoms and haptophytes to fibrillar callose from *Laminariales* (2,10) and granular paramylon from *Euglena* (3). Therefore, it is difficult to predict the true substrate of a β-1,3-glucanase just based on genome annotation. Moreover, some laminarinases from family GH16 are well known to be also active on mixed-linked glucans (38). The International Union of Biochemistry and Molecular Biology (IUBMB) distinguishes two EC numbers for laminarinases: EC 3.2.1.39 describes the enzymes strictly specific for β-1,3-glucan, and EC 3.2.1.6 refers to glycoside hydrolases cleaving either 1,3-β-glucans or the β-1,4 linkage in 1,3-1,4-β-glucans. While EC 3.2.1.39 enzymes are found in several GH families (GH16, GH17, GH55, GH64, GH81 and GH128), EC 3.2.1.6 enzymes have been only described in GH16 family to date (38). However, the EC nomenclature does not take into account the structural diversity of 1,3-β-glucans and in the literature enzymes referred to as laminarinases are not always tested on other substrates, such as MLG, which may lead to incorrect EC number assignment.

In this context, we have characterized the structure and specificity of *Zg*LamA, one of the five putative laminarinases found in the genome of *Z. galactanivorans*. *Zg*LamA$_{GH16}$ is an endolytic β-glucanase highly efficient for the degradation of algal laminarin, but has no significant activity on semi-crystalline 1,3-β-glucans such as curdlan and paramylon. Its minimal substrate is laminaritriose, releasing glucose and laminaribiose. *Zg*LamA$_{GH16}$ has also a residual activity on MLG from barley, but its catalytic efficiency on this polysaccharide is 22 fold inferior in comparison to laminarin. The structure of *Zg*LamA$_{GH16-E269S}$ in complex with MLG trisaccharide (G4G3G) reveals that the β-1,3 glycosidic bond is localized between subsites -1 and -2. Consistently, our FACE analysis of the hydrolysis of the commercial tetrasaccharide G4G3G4G has demonstrated that *Zg*LamA$_{GH16}$ specifically cleaves β-1,4 linkages next to β-1,3 linkages (Fig. 3D). Due to its residual activity on MLG, *Zg*LamA$_{GH16}$ is thus formally assigned the

EC number 3.2.1.6, although its efficiency is much higher on laminarin. This highlights the limits of the EC nomenclature. Interestingly, the laminarinase *Rm*LamR from *R. marinus*, which is relatively similar to *Zg*LamA$_{GH16}$ (41% identity), is in fact ~5 fold more active on MLG than on laminarin (specific activities: 3111 U/mg and 656 U/mg) (52).

How did such a remarkable difference in substrate specificity develop for two closely related enzymes? The comparison of the structure of *Zg*LamA$_{GH16}$ to *Rm*LamR (35) gives rise to an obvious explanation. The succession of β-1,3 bonds gives to laminarin a helical conformation (Fig. 4E). In contrast, MLG has a linear shape (Fig. 4F), due to its fine structure dominated by the presence of β-1,4 linkages (~70%) and irregular interruptions of single β-1,3 bonds (53). The external rim of the *Rm*LamR sugar-binding cleft is parallel to the inner β-sheet, resulting in a straight groove, which is well suited for binding linear MLG (Fig. 4D). In contrast, *Zg*LamA$_{GH16}$ displays an additional loop which precludes the binding of a polysaccharide parallel to the β-sheets. Instead, this additional loop provides a bend in the active site of the enzyme (Fig. 4C), which is complimentary to the helical conformation of laminarin (Fig. 4E), explaining the high efficiency of *Zg*LamA$_{GH16}$ on 1,3-β-glucans and its limited activity on MLG.

The comparison of the complexes of *Zg*LamA$_{GH16\text{-}E269S}$, *Pc*Lam16A and TFsβ-glucanase highlights other crucial differences in the molecular recognition of laminarin and MLG by these various GH16 β-glucanases. Like *Rm*LamR, the fungal laminarinase *Pc*Lam16A displays a quite straight cleft, consistent with its broad specificity for curdlan, laminarin and MLG (40,54). The mode of laminarin recognition is partially shared between *Zg*LamA$_{GH16\text{-}E269S}$ and *Pc*Lam16A, but it is limited to the subsites -1 and -2 (Fig. 5). Moreover, *Zg*LamA$_{GH16\text{-}E269S}$ binds the glucose unit in subsite -2 more tightly than *Pc*Lam16A, with three additional amino acids involved in the recognition. *Zg*LamA$_{GH16}$ displays a larger interaction surface due to a third negative subsite (absent in *Pc*Lam16A), which thus increases the affinity of this enzyme for laminarin. TFsβ-glucanase and *Zg*LamA$_{GH16}$ have been both crystallized with a trisaccharide G4G3G, but they only share a partially conserved subsite -1 in common (Fig.6) . The groove of TFsβ-glucanase is with a straight topology, well adapted to bind linear MLG. A similar binding in *Zg*LamA$_{GH16}$ would provoke a steric clash between the oligosaccharide and the additional loop of this laminarinase. Thus, though these GH16 enzymes bind the same substrate they essentially differ in their interaction with MLG.

Conclusion

Phylogenetic and structural evidences support that the common ancestor of the GH16 family featured a β-bulge between the conserved catalytic residues and was likely a β-1,3-glucanase (49,55). This hypothesis is consistent with the fact that 1,3-β-glucan is an ancestral storage polysaccharide in eukaryotes (2) and thus a very ancient source of carbon for marine bacteria. Nonetheless, numerous laminarinases in the family GH16 hydrolyze both 1,3-β-glucans and MLG. This is the case of the other GH16 laminarinases which have been structurally characterized (Fig. 1B). These enzymes display a straight catalytic groove, which easily fits a linear polysaccharide such as MLG. In contrast, *Zg*LamA is highly efficient for the degradation of laminarin and has only a residual activity on MLG. The presence of a unique loop in *Zg*LamA (Fig. 1) results in a bend in the active groove more adapted to the helical shape of laminarin (Fig. 4C,E). This bent topology is a simple alteration of the straight groove and appears as a relatively low cost evolution towards a greater specificity for laminarin. Altogether, we propose that the ancestral laminarinases in family GH16 had a broad specificity for both laminarin and MLG. The emergence of GH16 enzymes that are more specific and efficient for the degradation of laminarin is likely a more recent evolutionary event. A phylogenetic analysis of the close homologues of *Zg*LamA$_{GH16}$ and *Rm*LamR and of characterized laminarinases strengthens this hypothesis. Indeed *Zg*LamA$_{GH16}$ forms a solid clade with 12 laminarinases (Fig. 7). The additional loop is conserved in these 12 enzymes (data not shown). The clade comprising *Zg*LamA$_{GH16}$ is rooted by several clades of laminarinases which do not possess with this

specific loop (Fig. 7). These latter GH16 enzymes likely have a straight groove as observed for the structurally characterized laminarinases (PDB: 2VY0, 3AZX, 3ATG, 2HYK, 3ILN, 2CL2). Therefore, the *Zg*LamA$_{GH16}$ clade emerged more recently than the clades of laminarinases with straight groove. Such a hypothesis is also already accepted for the evolution of GH16 enzymes more specific for MLG. Indeed, bacterial lichenases (EC 3.2.1.73) have lost the β-bulge of the ancestral catalytic center (conserved in most clan GH-B enzymes: all GH7 and most GH16 enzymes), and thus diverge later from β-1,3-glucanases (49). Interestingly, a new GH16 enzyme from black cottonwood, *Pt*EG16, has been recently characterized as a broad specificity β-glucanase with a nearly equal capacity to hydrolyze MLG and xyloglucans. This new subfamily has been proposed as a key evolutionary intermediate between lichenases and XET/xyloglucanases (56). For us, the discovery of *Pt*EG16 also indicates that the MLG degradation activity has emerged at least three times within the family GH16 (broad specificity laminarinases, lichenases and EG16). Altogether, our characterization of *Zg*LamA and the recent results from Harry Brumer and coworkers (56) emphasize the complex and bumpy history of this fascinating GH family and that the evolution between broad and narrow substrate specificity can be back and forth.

ACKNOWLEDGMENTS

This work was supported by the French National Research Agency with regards to the investment expenditure program IDEALG (http://www.idealg.ueb.eu/, grant agreement No. ANR-10-BTBR-04,). The PhD fellowship of A.L. was funded by French Ministry of Higher Education and Research. We are indebted to local contacts for their support during data collection at beamlines ID23-1 and ID29, ESRF (European synchrotron, Grenoble, France). We also thank Dr. Elizabeth Ficko-Blean for helpful discussion and critical reading of our manuscript.

REFERENCES

1. Stone, B. A. (2009) Chemistry of β-glucans. in *Chemistry, biochemistry and biology of (1->3)-β-glucans and related polysaccharides* (Bacic, A., Fincher, G. B., and Stone, B. A. eds.), Academic Press. pp 5-46
2. Michel, G., Tonon, T., Scornet, D., Cock, J. M., and Kloareg, B. (2010) Central and storage carbon metabolism of the brown alga *Ectocarpus siliculosus*: insights into the origin and evolution of storage carbohydrates in Eukaryotes. *New Phytol.* **188**, 67-81
3. Clarke, A. E., and Stone, B. A. (1960) Structure of the paramylon from *Euglena gracilis*. *Biochim. Biophys. Acta* **44**, 161-163
4. Janse, I., van Rijssel, M., van Hall, P. J., Gerwig, G. J., Gottschal, J. G., and Prius, R. A. (1996) The storage glucan of *Phaeocystis globosa* (*Prymnesiophyceae*) cells. *J.Phycol.* **32**, 382–387
5. Hirokawa, Y., Fujiwara, S., Suzuki, M., Akiyama, T., Sakamoto, M., Kobayashi, S., and Tsuzuki, M. (2008) Structural and physiological studies on the storage beta-polyglucan of haptophyte *Pleurochrysis haptonemofera*. *Planta* **227**, 589-599
6. Beattie, A., Hirst, E. L., and Percival, E. (1961) Studies on the metabolism of the Chrysophyceae. Comparative structural investigations on leucosin (chrysolaminarin) separated from diatoms and laminarin from the brown algae. *Biochem. J.* **79**, 531-537
7. Wang, M. C., and Bartnicki-Garcia, S. (1974) Mycolaminarans: storage (1,3)-β-D-glucans from the cytoplasm of the fungus *Phytophthora palmivora*. *Carbohydr. Res.* **37**, 331-338
8. Percival, E. G. V., and Ross, A. G. (1951) The constitution of laminarin. Part II. The soluble laminarin of *Laminaria digitata*. *J. Chem. Soc.*, 720 - 726
9. Read, S. M., Currie, G., and Bacic, A. (1996) Analysis of the structural heterogeneity of laminarin by electrospray-ionisation-mass spectrometry. *Carbohydr. Res.* **281**, 187-201

10. Michel, G., Tonon, T., Scornet, D., Cock, J. M., and Kloareg, B. (2010) The cell wall polysaccharide metabolism of the brown alga *Ectocarpus siliculosus*. Insights into the evolution of extracellular matrix polysaccharides in Eukaryotes. *New Phytol.* **188**, 82-97
11. Smith, S. V. (1981) Marine Macrophytes as a Global Carbon Sink. *Science* **211**, 838-840
12. Duarte, C. M., Middelburg, J. J., and Caraco, N. (2005) Major role of marine vegetation on the oceanic carbon cycle. *Biogeosciences* **2**, 1-8
13. Siegel, D. A., Doney, S. C., and Yoder, J. A. (2002) The North Atlantic spring phytoplankton bloom and Sverdrup's critical depth hypothesis. *Science* **296**, 730-733
14. Cloern, J. E. (1996) Phytoplankton bloom dynamics in coastal ecosystems: a review with some general lessons from sustained investigation of San Francisco Bay, California. *Rev. Geophys.* **34**, 127-168
15. DiTullio, G. R., Grebmeier, J. M., Arrigo, K. R., Lizotte, M. P., Robinson, D. H., Leventer, A., Barry, J. P., VanWoert, M. L., and Dunbar, R. B. (2000) Rapid and early export of *Phaeocystis antarctica* blooms in the Ross Sea, Antarctica. *Nature* **404**, 595-598
16. Alderkamp, A. C., van Rijssel, M., and Bolhuis, H. (2007) Characterization of marine bacteria and the activity of their enzyme systems involved in degradation of the algal storage glucan laminarin. *FEMS Microbiol. Ecol.* **59**, 108-117
17. Arnosti, C., Fuchs, B. M., Amann, R., and Passow, U. (2012) Contrasting extracellular enzyme activities of particle-associated bacteria from distinct provinces of the North Atlantic Ocean. *Front. Microbiol.* **3**, 425
18. Teeling, H., Fuchs, B. M., Becher, D., Klockow, C., Gardebrecht, A., Bennke, C. M., Kassabgy, M., Huang, S., Mann, A. J., Waldmann, J., Weber, M., Klindworth, A., Otto, A., Lange, J., Bernhardt, J., Reinsch, C., Hecker, M., Peplies, J., Bockelmann, F. D., Callies, U., Gerdts, G., Wichels, A., Wiltshire, K. H., Glockner, F. O., Schweder, T., and Amann, R. (2012) Substrate-controlled succession of marine bacterioplankton populations induced by a phytoplankton bloom. *Science* **336**, 608-611
19. Thomas, F., Hehemann, J. H., Rebuffet, E., Czjzek, M., and Michel, G. (2011) Environmental and gut bacteroidetes: the food connection. *Front. Microbiol.* **2**, 93
20. Barbeyron, T., L'Haridon, S., Corre, E., Kloareg, B., and Potin, P. (2001) *Zobellia galactanovorans* gen. nov., sp. nov., a marine species of *Flavobacteriaceae* isolated from a red alga, and classification of. *Int. J. Syst. Evol. Microbiol.* **51**, 985-997
21. Hehemann, J. H., Correc, G., Barbeyron, T., Helbert, W., Czjzek, M., and Michel, G. (2010) Transfer of carbohydrate-active enzymes from marine bacteria to Japanese gut microbiota. *Nature* **464**, 908-912
22. Rebuffet, E., Groisillier, A., Thompson, A., Jeudy, A., Barbeyron, T., Czjzek, M., and Michel, G. (2011) Discovery and structural characterization of a novel glycosidase family of marine origin. *Environ. Microbiol.* **13**, 1253-1270
23. Hehemann, J. H., Correc, G., Thomas, F., Bernard, T., Barbeyron, T., Jam, M., Helbert, W., Michel, G., and Czjzek, M. (2012) Biochemical and Structural Characterization of the Complex Agarolytic Enzyme System from the Marine Bacterium *Zobellia galactanivorans*. *J. Biol. Chem.* **287**, 30571-30584
24. Barbeyron, T., Michel, G., Potin, P., Henrissat, B., and Kloareg, B. (2000) iota-Carrageenases constitute a novel family of glycoside hydrolases, unrelated to that of kappa-carrageenases. *J. Biol. Chem.* **275**, 35499-35505
25. Rebuffet, E., Barbeyron, T., Jeudy, A., Jam, M., Czjzek, M., and Michel, G. (2010) Identification of catalytic residues and mechanistic analysis of family GH82 iota-carrageenases. *Biochemistry* **49**, 7590-7599
26. Thomas, F., Barbeyron, T., Tonon, T., Genicot, S., Czjzek, M., and Michel, G. (2012) Characterization of the first alginolytic operons in a marine bacterium: from their emergence in marine *Flavobacteriia* to their independent transfers to marine *Proteobacteria* and human gut *Bacteroides*. *Environ. Microbiol.* **14**, 2379-2394

27. Thomas, F., Lundqvist, L. C., Jam, M., Jeudy, A., Barbeyron, T., Sandstrom, C., Michel, G., and Czjzek, M. (2013) Comparative characterization of two marine alginate lyases from *Zobellia galactanivorans* reveals distinct modes of action and exquisite adaptation to their natural substrate. *J. Biol. Chem.* **288**, 23021-23037
28. Groisillier, A., Herve, C., Jeudy, A., Rebuffet, E., Pluchon, P. F., Chevolot, Y., Flament, D., Geslin, C., Morgado, I. M., Power, D., Branno, M., Moreau, H., Michel, G., Boyen, C., and Czjzek, M. (2010) MARINE-EXPRESS: taking advantage of high throughput cloning and expression strategies for the post-genomic analysis of marine organisms. *Microb. Cell Fact.* **9**, 45
29. Studier, F. W. (2005) Protein production by auto-induction in high density shaking cultures. *Protein. Expr. Purif.* **41**, 207-234
30. Kidby, D. K., and Davidson, D. J. (1973) A convenient ferricyanide estimation of reducing sugars in the nanomole range. *Anal. Biochem.* **55**, 321-325
31. Jackson, P. (1990) The use of polyacrylamide-gel electrophoresis for the high-resolution separation of reducing saccharides labelled with the fluorophore 8-aminonaphthalene-1,3,6-trisulphonic acid. Detection of picomolar quantities by an imaging system based on a cooled charge-coupled device. *Biochem. J.* **270**, 705-713
32. Leslie, A. G. (2006) The integration of macromolecular diffraction data. *Acta Crystallogr. D* **62**, 48-57
33. Weiss, M. S., Sicker, T., Djinovic-Carugo, K., and Hilgenfeld, R. (2001) On the routine use of soft X-rays in macromolecular crystallography. *Acta Crystallogr. D* **57**, 689-695
34. Vagin, A., and Teplyakov, A. (1997) MOLREP: an Automated Program for Molecular Replacement. *J. Appl. Crystallogr.* **30**, 1022-1025
35. Bleicher, L., Prates, E. T., Gomes, T. C., Silveira, R. L., Nascimento, A. S., Rojas, A. L., Golubev, A., Martinez, L., Skaf, M. S., and Polikarpov, I. (2011) Molecular basis of the thermostability and thermophilicity of laminarinases: X-ray structure of the hyperthermostable laminarinase from *Rhodothermus marinus* and molecular dynamics simulations. *J. Phys. Chem. B* **115**, 7940-7949
36. Emsley, P., Lohkamp, B., Scott, W. G., and Cowtan, K. (2010) Features and development of Coot. *Acta Crystallogr. D* **66**, 486-501
37. Vagin, A. A., Steiner, R. A., Lebedev, A. A., Potterton, L., McNicholas, S., Long, F., and Murshudov, G. N. (2004) REFMAC5 dictionary: organization of prior chemical knowledge and guidelines for its use. *Acta Crystallogr. D* **60**, 2184-2195
38. Cantarel, B. L., Coutinho, P. M., Rancurel, C., Bernard, T., Lombard, V., and Henrissat, B. (2009) The Carbohydrate-Active EnZymes database (CAZy): an expert resource for Glycogenomics. *Nucleic Acids Res.* **37**, D233-238
39. Katoh, K., and Standley, D. M. (2013) MAFFT multiple sequence alignment software version 7: improvements in performance and usability. *Mol. Biol. Evol.* **30**, 772-780
40. Vasur, J., Kawai, R., Andersson, E., Igarashi, K., Sandgren, M., Samejima, M., and Stahlberg, J. (2009) X-ray crystal structures of *Phanerochaete chrysosporium* Laminarinase 16A in complex with products from lichenin and laminarin hydrolysis. *FEBS J.* **276**, 3858-3869
41. Tsai, L. C., Shyur, L. F., Cheng, Y. S., and Lee, S. H. (2005) Crystal structure of truncated *Fibrobacter succinogenes* 1,3-1,4-beta-D-glucanase in complex with beta-1,3-1,4-cellotriose. *J Mol Biol* **354**, 642-651
42. Katoh, K., Misawa, K., Kuma, K., and Miyata, T. (2002) MAFFT: a novel method for rapid multiple sequence alignment based on fast Fourier transform. *Nucleic Acids Res.* **30**, 3059-3066
43. Tamura, K., Peterson, D., Peterson, N., Stecher, G., Nei, M., and Kumar, S. (2011) MEGA5: molecular evolutionary genetics analysis using maximum likelihood, evolutionary distance, and maximum parsimony methods. *Mol. Biol. Evol.* **28**, 2731-2739
44. Wang, Y. K., Zhao, G. Y., Li, Y., Chen, X. L., Xie, B. B., Su, H. N., Lv, Y. H., He, H. L., Liu, H., Hu, J., Zhou, B. C., and Zhang, Y. Z. (2010) Mechanistic insight into the function of the C-terminal PKD domain of the collagenolytic serine protease deseasin MCP-01 from deep sea

Pseudoalteromonas sp. SM9913: binding of the PKD domain to collagen results in collagen swelling but does not unwind the collagen triple helix. *J. Biol. Chem.* **285**, 14285-14291
45. Viladot, J. L., de Ramon, E., Durany, O., and Planas, A. (1998) Probing the mechanism of *Bacillus* 1,3-1,4-beta-D-glucan 4-glucanohydrolases by chemical rescue of inactive mutants at catalytically essential residues. *Biochemistry* **37**, 11332-11342
46. Davies, G. J., Wilson, K. S., and Henrissat, B. (1997) Nomenclature for sugar-binding subsites in glycosyl hydrolases. *Biochem. J.* **321**, 557-559
47. Johansson, P., Brumer, H., 3rd, Baumann, M. J., Kallas, A. M., Henriksson, H., Denman, S. E., Teeri, T. T., and Jones, T. A. (2004) Crystal structures of a poplar xyloglucan endotransglycosylase reveal details of transglycosylation acceptor binding. *Plant Cell* **16**, 874-886
48. Baumann, M. J., Eklof, J. M., Michel, G., Kallas, A. M., Teeri, T. T., Czjzek, M., and Brumer, H., 3rd. (2007) Structural evidence for the evolution of xyloglucanase activity from xyloglucan endo-transglycosylases: biological implications for cell wall metabolism. *Plant Cell* **19**, 1947-1963
49. Michel, G., Chantalat, L., Duee, E., Barbeyron, T., Henrissat, B., Kloareg, B., and Dideberg, O. (2001) The kappa-carrageenase of *P. carrageenovora* features a tunnel-shaped active site: a novel insight in the evolution of Clan-B glycoside hydrolases. *Structure* **9**, 513-525
50. Keitel, T., Meldgaard, M., and Heinemann, U. (1994) Cation binding to a Bacillus (1,3-1,4)-beta-glucanase. Geometry, affinity and effect on protein stability. *Eur. J. Biochem.* **222**, 203-214
51. Sulzenbacher, G., Driguez, H., Henrissat, B., Schülein, M., and davies, G. J. (1996) Structure of the *Fusarium oxysporum* Endoglucanase I with a Nonhydrolyzable Substrate Analogue: Substrate Distortion Gives Rise to the Preferred Axial Orientation for the Leaving Group. *Biochemistry* **35**
52. Krah, M., Misselwitz, R., Politz, O., Thomsen, K. K., Welfle, H., and Borriss, R. (1998) The laminarinase from thermophilic eubacterium *Rhodothermus marinus*--conformation, stability, and identification of active site carboxylic residues by site-directed mutagenesis. *Eur. J. Biochem.* **257**, 101-111
53. Woodward, J. R., Fincher, G. B., and Stone, B. A. (1983) Water-Soluble (1-->3), (1-->4)-β-D-Giucans from Barley (*Hordeum vulgate*) Endosperm. II. Fine Structure. *Carbohydr. Polym.* **3**, 207-225
54. Kawai, R., Igarashi, K., Yoshida, M., Kitaoka, M., and Samejima, M. (2006) Hydrolysis of beta-1,3/1,6-glucan by glycoside hydrolase family 16 endo-1,3(4)-beta-glucanase from the basidiomycete *Phanerochaete chrysosporium*. *Appl. Microbiol. Biotechnol.* **71**, 898-906
55. Barbeyron, T., Gerard, A., Potin, P., Henrissat, B., and Kloareg, B. (1998) The kappa-carrageenase of the marine bacterium *Cytophaga drobachiensis*. Structural and phylogenetic relationships within family-16 glycoside hydrolases. *Mol. Biol. Evol.* **15**, 528-537
56. Eklof, J. M., Shojania, S., Okon, M., McIntosh, L. P., and Brumer, H. (2013) Structure-Function Analysis of a Broad Specificity Populus trichocarpa Endo-beta-glucanase Reveals an Evolutionary Link between Bacterial Licheninases and Plant XTH Gene Products. *J. Biol. Chem.* **288**, 15786-15799
57. Gouet, P., Robert, X., and Courcelle, E. (2003) ESPript/ENDscript: Extracting and rendering sequence and 3D information from atomic structures of proteins. *Nucleic Acids Res.* **31**, 3320-3323

Tables

Table 1: Data collection and refinement statistics for the crystal structures of the native $LamA_{cat}$ and the mutant $LamA_{GH16\text{-}E269S}$ in complex with its substrates.

	$LamA_{cat}$	**$LamA_{GH16\text{-}E269S}$-laminarin**	**$LamA_{GH16\text{-}E269S}$-MLG**
Data collection			
Beamline	ID23-1	ID29	
Wavelenght	0.979	0.976	
Space group	$P2_12_12_1$	$P2_12_12_1$	$P2_12_12_1$
Unit cell	a=44.55 Å ; b=76.56 Å; c=142.10 Å α=β=γ=90°	a=44.46 Å ; b=76.50 Å; c=142.94 Å α=β=γ=90°	a=44.53 Å ; b=76.49 Å; c=142.67 Å α=β=γ=90°
Resolution range [a] (Å)	47.37-1.45 (1.53-1.45)	40.44-1.35 (1.42-1.35)	47.56-1.13 (1.19-1.13)
Total data	549758	505574	894665
Unique data	86903	107451	181382
Completeness (%)	99.70 (99.30)	99.70 (99.70)	99.20 (95.70)
Mean I/σ(I)	11 (3.50)	16.3 (2.30)	10.5 (1.90)
[b]R_{sym} ; [c]R_{pim}(%)	10.1 (45.5); 4.4 (20.7)	4.5 (54.6); 2.3 (27.4)	6.9 (65.9); 3.3 (22.7)
Redundancy	6.3	4.7	4.9
Refinement statistics			
Resolution range	42.52-1.50 (1.54-1.50)	38.44-1.35 (1.42-1.35)	42.51-1.13 (1.16-1.13)
Unique reflexions	74179 (5145)	102000 (7079)	172173 (11168)
Reflexions R_{free}	3929 (273)	5366 (354)	9107 (597)
R / R_{free} (%)	13.9/16.6 (18.7/23.3)	13.2/16.7 (21.2/25.3)	14.4/17.5 (28.0/29.8)
RMSD bond lengths	0.028 Å	0.026 Å	0.026 Å
RMSD bond angles	2.29°	2.32°	2.3°
Overall B factor (Å²)	18.16	23.55	20.32
B factor: Molecule A (Å²)	14.18	18.44	17.26
B factor: Molecule B (Å²)	19.83	25.72	20.52
B factor: Solvant (Å²)	27.19	34.67	30.87
B factor: Ligands (Å²)	-	(A) 19.27. (B) 26 .88	(A) 17.42. (B) 21.80
PDB ID			
	4BQ1	4BOW	4BPZ

[a]Values in parentheses concern the high resolution shell.

[b] $R_{sym} = \Sigma \mid I\text{-}I_{av} \mid / \Sigma \mid I \mid$, where the summation is over all symmetry-equivalent reflections.

[c] R_{pim} = corresponds to the multiplicity weighted R_{sym}.

Figure Legends

Figure 1: Modular architecture of *Zg*LamA (A) and structure-based sequence alignment of family GH16 laminarinases (B). (A) LP=lipoprotein signal peptide suggesting that ZgLamA is anchored in the outer membrane. In the N-terminal region, the signal peptide is followed by a Polycysitic Kidney Disease (PKD)-like module composed of 102 residues. The C-terminal region is composed of a catalytic module of glycoside hydrolase family 16 (GH16). (B) ***Zg***LamA$_{GH16}$ is compared with all the laminarinases structurally characterized so far. Alpha helices and beta strands are represented as helix and arrows respectively, and beta turn are maked with TT. This sequence alignment was created using the following sequences from the Protein Data Bank; Laminarinase 16A from *Phanerochaete chrysosporium* (2W39, residues 1-298), LamR from *Rhodothermus marinus* (3ILN, residues 2-249), BglF from *Nocardiopsis sp. F96* (2HYK, residues 4-244), endo-1,3-beta-glucanase from *Cellulosimicrobium cellulans* (3ATG, residues 1-255), TM_0024 from *Thermogota maritima* (3AZX, residues 7-256), Tpet_0899 from *Thermotoga petrophila* (4DFS, residues 15-264), LamA from *Pyrococcus furiosus* (2VY0, residues 10-261), endo-1,3-beta-glucanase from *Streptomyces sioyaensis* (3DGT, residues 6-276). Dark shaded boxes enclose invariant positions, and light shaded boxes show positions with similar residues. The figure was created with ESPript (57).

Figure 2: Effect of the pH on the activity of ZgLamAGH16 (A) and Michaelis-Menten kinetics with its two substrates (B). (A) The experiments were undertaken at 40°C in buffer 100 mM, with 10 nM of purified enzyme and 0.06% (w/v) of laminarin. The activity in buffer glycine-NaOH pH 8.5 was used considered as reference for the activity maximum. (B) The experiments were undertaken with 10 nM of *Zg*LamA$_{GH16}$ at 40°C in 100 mM glycine buffer pH 8.5. For each substrate, five concentrations were used: 0.06% (w/v), 0.12%, 0.24%, 0.48%, and 0.96% for laminarin; 0.05% (w/v), 0.1%, 0.15%, 0.2% and 0.25% for MLG. Aliquots of the reaction mixture were taken every 2 min over 10 min for laminarin and every 15 min over 1 h for mixed linked glucan (MLG).

Figure 3: Mode of action and terminal products of *Zg*LamA$_{GH16}$. Hydrolysis of laminarin (A, C) and mixed linked glucan (MLG) (B, D) by *Zg*LamA$_{GH16}$ were monitored by Fluorophore Assisted Carbohydrate Electrophoresis (FACE). (A) 0.5% (w/v) of laminarin was hydrolyzed by 100 nM of *Zg*LamA$_{GH16}$ at 20°C. (B) 0.5% (w/v) of MLG was hydrolyzed by 4.5 µM of *Zg*LamA$_{GH16}$ at 40°C. (C) Standard laminarin oligosaccharides are labelled from DP2 to DP6 (Lane 1, 2, 4, 6 and 8). 100 µg at 0.1% of the oligosaccharides from DP3 to DP6 were incubated with 4.5 µM of *Zg*LamA$_{GH16}$ at 37°C for 12 hours (Lane 3, 5, 7 and 9). (D) The reaction mixtures contain 0.1% (w/v) of the tetrasaccharide (G4G3G4G) and 4.5 µM of active (lane 3 and 5) or inactive (lane 4) *Zg*LamA$_{GH16}$ in glycine buffer pH 8.5 at 37°C for 30 min. The asterisk indicates that the G4G3G4G oligosaccharides were labelled before the enzymatic reaction, while the absence of asterisk indicates that the oligosaccharides were labelled after the reaction.

Figure 4: *Zg*LamA$_{GH16}$ displays a bent topology adapted to the binding of helical-shaped laminarin. (A)**.** Fold representation of *Zg*LamA$_{GH16}$ in complex with a laminarin tetrasaccharide. The β-strands are represented by arrows. The additional loop of *Zg*LamA$_{GH16}$ is colored in red. (B) Fold representation of *Rm*LamR from *Rhodothermus marinus*. (PDB code: 3ILN). (C) Stereo view of the surface of *Zg*LamA$_{GH16}$ highlighting the bent topology of the active groove (green arrow). The orientations of *Zg*LamA$_{GH16}$ are identical in A and C. (D) Stereo view of the surface of *Rm*LamR highlighting its straight cleft topology (green arrow). The orientations of *Rm*LamR are identical in B and D. (E) The laminarihexaose bound to the CBM6 of *Bacillus halodurans* (PDB code 1W9W) adopts a helical conformation due to its β-1,3-linkages. (F) The tetrasaccharide of MLG (G4G3G4G) bound to the CBM6 of *Cellvibrio mixtus* (PDB accession code 1UZ0) adopts a linear conformation due to the alternation of β-1,4- and β-1,3-linkages.

Figure 5: Molecular basis for laminarin recognition by *Zg*LamA$_{GH16-E269S}$. (A). Schematic representation of *Zg*LamA$_{GH16-E269S}$ bound to a laminaritetraose (G3G3G3G). The dotted lines and the double arrows represent hydrogen bonds and hydrophobic stackings, respectively. (B,C) Structural comparison of the laminarinases *Zg*LamA$_{GH16-E269S}$ (B) and *Pc*Lam16A from the terrestrial fungus *Phanerochaete chrysosporium (C)* bound to laminarin oligosaccharides (G3G3G3G and G3G, respectively). *Pc*Lam16A (PDB code 2W39) has 27% identity with *Zg*LamA$_{GH16}$. The amino-acids are colored as follows; in red, the catalytic residues conserved in the family GH16; in purple, the residues involved in laminarin recognition conserved between the two proteins; in blue, the residues which differ in the recognition pattern. The asterisk refers to the mutation of the Glu269 into a Ser269 in *Zg*LamA$_{GH16-E269S}$.

Figure 6: Molecular basis for mixed linked glucan (MLG) recognition by *Zg*LamA$_{GH16-E269S}$. (A) Schematic representation of *Zg*LamA$_{GH16-E269S}$ bound to a MLG trisaccharide G4G3G. The dotted lines and the double arrows represent hydrogen bonds and hydrophobic stackings, respectively. (B,C) Structural comparison of the laminarinase *Zg*LamA$_{GH16-E269S}$ (B) and the lichenase TFsβ-glucanase from *Fibrobacter succinogenes* (C) bound to a MLG trisaccharide (G4G3G). TFsβ-glucanase (PDB code 1ZM1) has 23% identity with *Zg*LamA$_{GH16}$. The amino-acids are colored as follows; in red, the catalytic residues conserved in the family GH16; in purple, the residues involved in MLG recognition conserved between the two proteins; in blue, the residues which differ in the recognition pattern. The asterisk refers to the mutation of the Glu269 into a Ser269 in *Zg*LamA$_{GH16-E269S}$.

Figure 7: Unrooted phylogenetic tree of the *Zg*LamA$_{GH16}$ homologues. The phylogenetic tree was derived using the Maximum Likelihood (ML) approach with the program MEGA5 (43). Numbers indicate the bootstrap values in the ML analysis. The sequences marked by black diamonds correspond to characterized laminarinases. The sequences used are listed below (with the following information: label, genbank accession number, organism): ZgLamA$_{GH16}$, CAZ96583, *Zobellia galactanivorans* Dsij; FscgcGH16, WP_020081599, *Flavobacterium* sp. SCGC AAA160-P02; NdGH16, YP_007376876, *Nonlabens dokdonensis* DSW-6; Fbal38GH16, WP_008253474, Flavobacteria bacterium BAL38; PfGH16, WP_018942276, *Polaribacter franzmannii*; LcGH16, WP_020536539, *Lewinella cohaerens*; Fms220GH16, WP_017842933, *Flavobacterium* sp. MS220-5C; Pmed152GH16, YP_007672281, *Polaribacter* sp. MED152; Fp7-3-5GH16, WP_019386462, Flavobacteriaceae bacterium P7-3-5; GlGH16, WP_006989208, *Gillisia limnaea*; Mhtcc2170GH16, YP_003862726, *Maribacter* sp. HTCC2170; Gck-I2-15GH16, WP_008992711, *Galbibacter* sp. ck-I2-15; MrGH16, YP_004787302, *Muricauda ruestringensis* DSM 13258; LbGH16, WP_009779440, *Leeuwenhoekiella blandensis*, FaGH16, CDF79586, *Formosa agariphila* KMM 3901, FbGH16, YP_004843635, *Flavobacterium branchiophilum* FL-15; MpGH16, WP_008508048, *Mucilaginibacter paludis*; AsGH16, WP_016194601, *Arcticibacter svalbardensis*; Cb6GH16, WP_022831977, Cytophagales str. B6; PfLam16_2VY0; AAC25554, *Pyrococcus furiosus* DSM 3638; TmLam16_3AZX, AAD35118, *Thermotoga maritima* MSB8; CcBglII_3ATG, AAC38290, *Cellulosimicrobium cellulans*; Nf96_BglF_2HYK, BAE54302, *Nocardiopsis* sp. F96; SlGH16, YP_003386191, *Spirosoma linguale* DSM 74; FlGH16, WP_009280395, *Fibrisoma limi*; FaesGH16, YP_007322050, *Fibrella aestuarina* BUZ 2; RaGH16, WP_017930206, *Robiginitomaculum antarcticum*; SlonGH16, WP_022834864, *Salisaeta longa*; SrGH16, YP_003572933, *Salinibacter ruber* M8; RmLamR_3ILN, AAC69707, *Rhodothermus marinus*; HnGH16, WP_022826080, *Hymenobacter norwichensis*; RpGH16, WP_019597521, *Rhodonellum psychrophilum*; MsGH16, WP_008629242, *Mariniradius saccharolyticus*; Apr1GH16, WP_008202826, *Algoriphagus* sp. PR1; HoGH16, YP_002508023, *Halothermothrix orenii* H 168; MsalGH16, WP_010663693, *Marinilabilia salmonicolor*; LbysGH16, YP_003996482, *Leadbetterella byssophila* DSM 17132, EpGH16, WP_018472769, *Echinicola pacifica*, and PcLam16A_2CL2, BAC67687, *Phanerochaete chrysosporium* K-3.

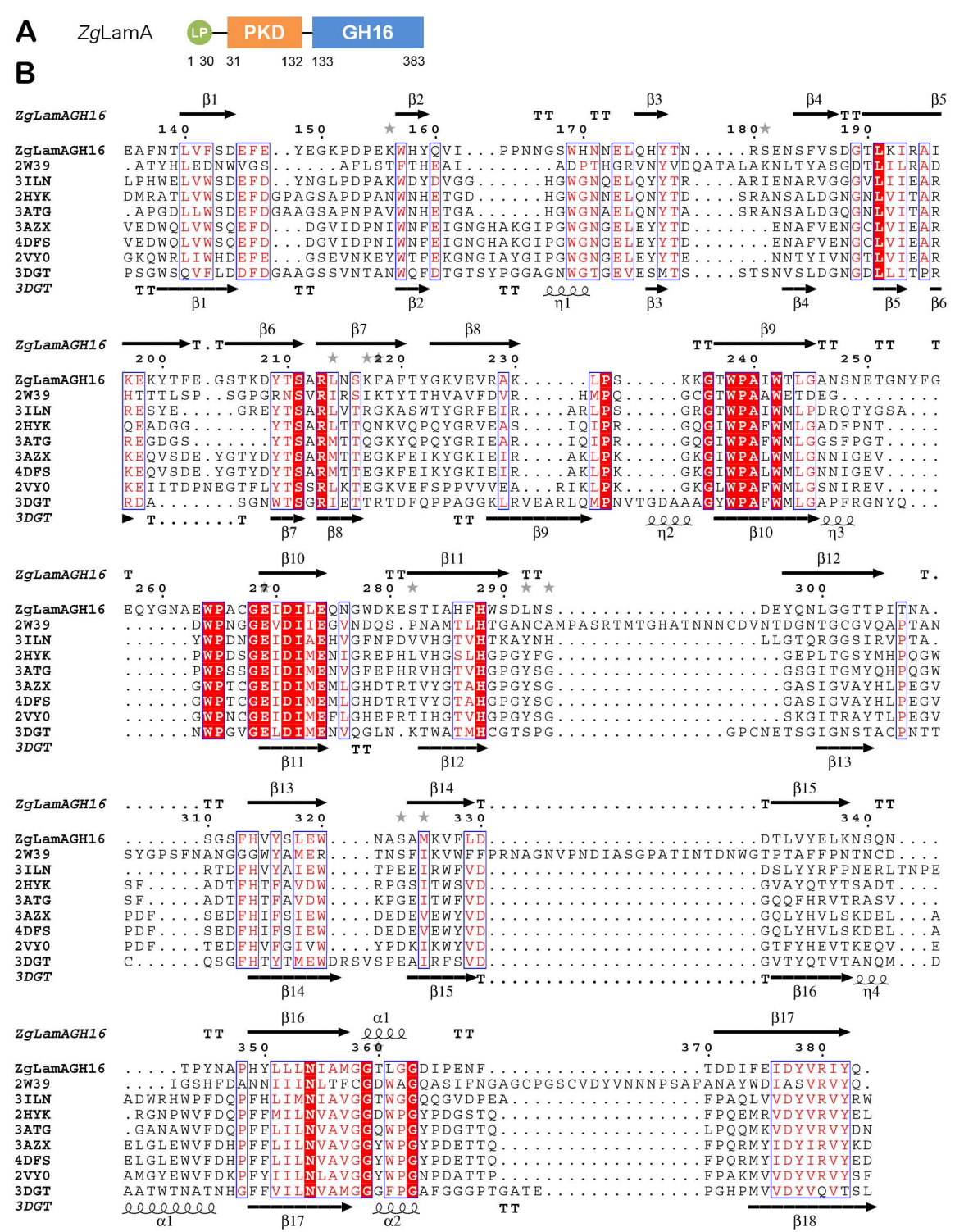
A
ZgLamA
LP
PKD
GH16
1 30 31 132 133 383
B
ZgLamAGH16
2W39
3ILN
2HYK
3ATG
3AZX
4DFS
2VY0
3DGT
3DGT

Figure 1

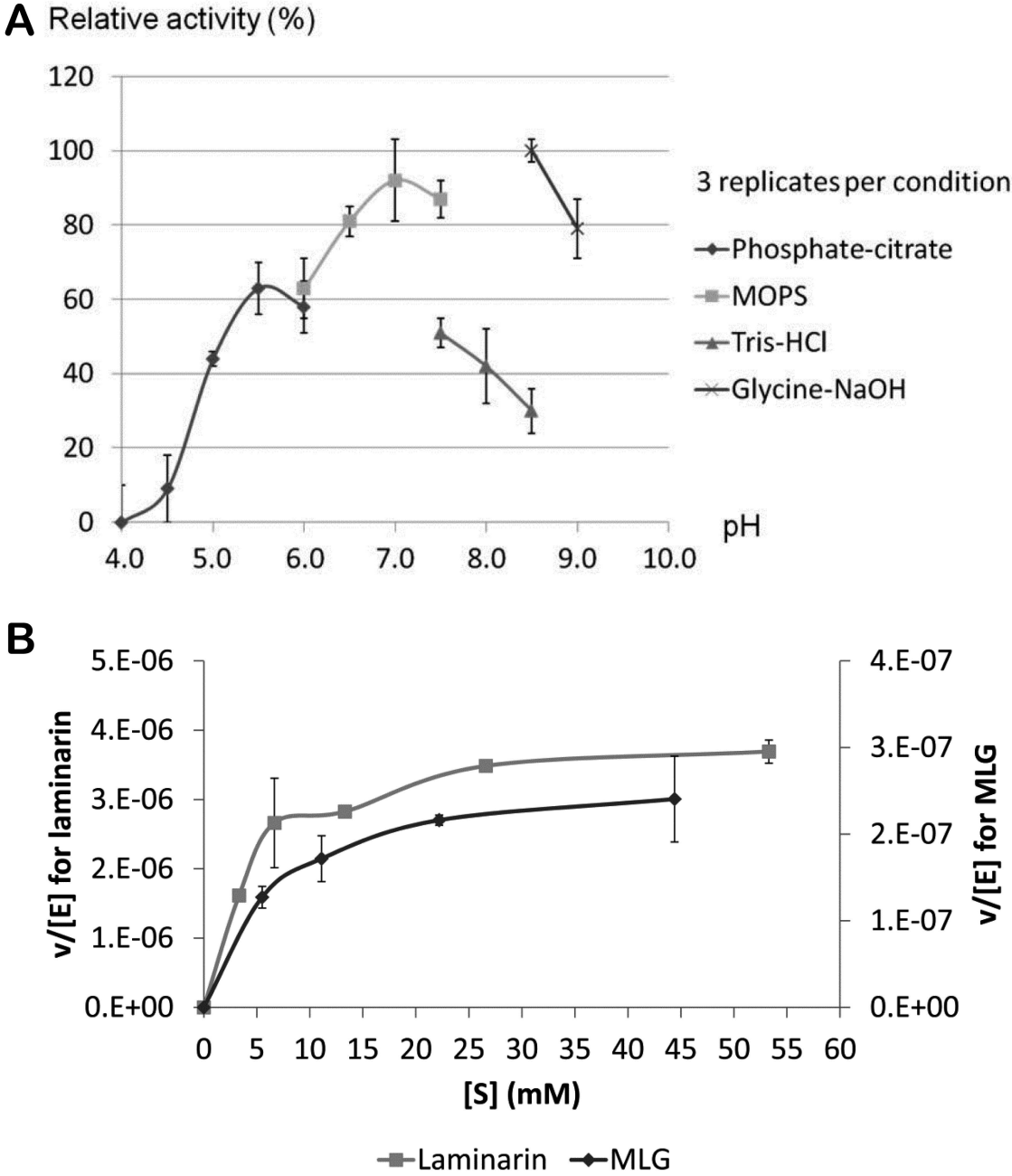
A
Relative activity (%)
120
100
80
60
40
20
0
4.0
5.0
6.0
7.0
8.0
9.0
10.0
pH
3 replicates per condition
Phosphate-citrate
MOPS
Tris-HCl
Glycine-NaOH
B
v/[E] for laminarin
5.E-06
4.E-06
3.E-06
2.E-06
1.E-06
0.E+00
v/[E] for MLG
4.E-07
3.E-07
2.E-07
1.E-07
0.E+00
0 5 10 15 20 25 30 35 40 45 50 55 60
[S] (mM)
Laminarin
MLG

Figure 2

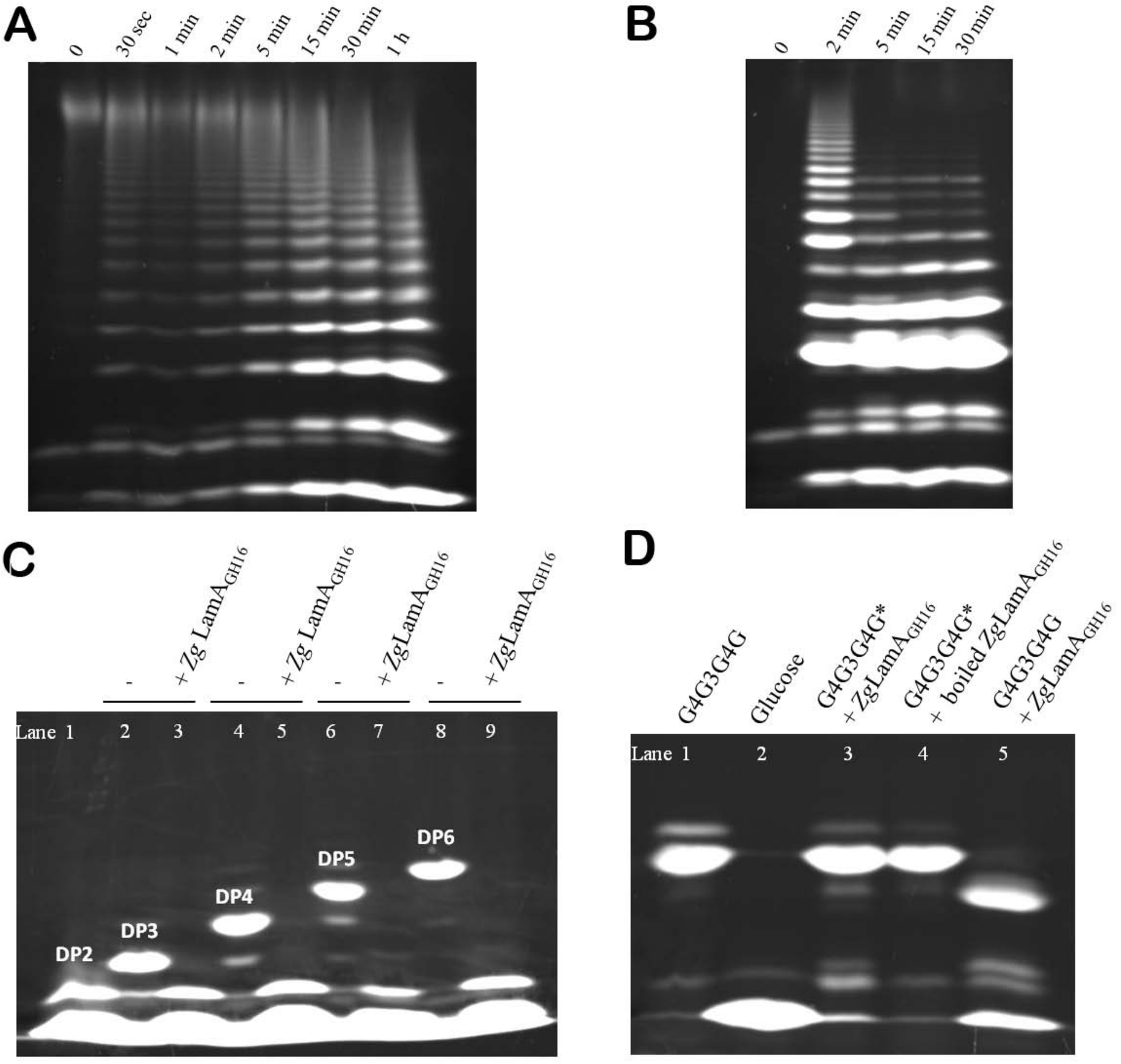
A
0
30 sec
1 min
2 min
5 min
15 min
30 min
1 h
B
0
2 min
5 min
15 min
30 min
C
-
+ Zg LamA$_{GH16}$
-
+ Zg LamA$_{GH16}$
-
+ ZgLamA$_{GH16}$
-
+ ZgLamA$_{GH16}$
Lane 1 2 3 4 5 6 7 8 9
DP2
DP3
DP4
DP5
DP6
D
G4G3G4G
Glucose
G4G3G4G*
+ ZgLamA$_{GH16}$
G4G3G4G*
+ boiled ZgLamA$_{GH16}$
G4G3G4G
+ ZgLamA$_{GH16}$
Lane 1 2 3 4 5

Figure 3

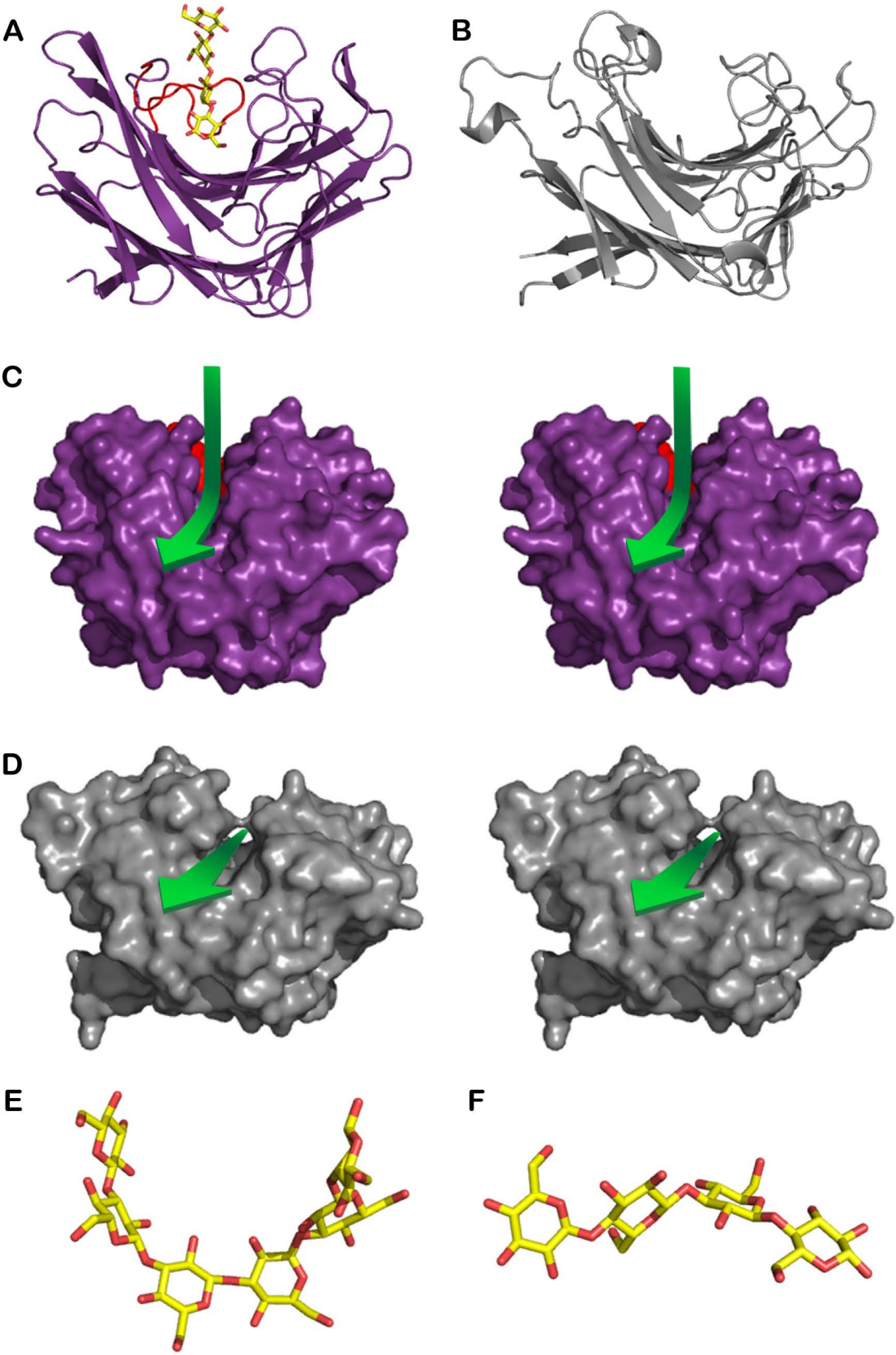

Figure 4

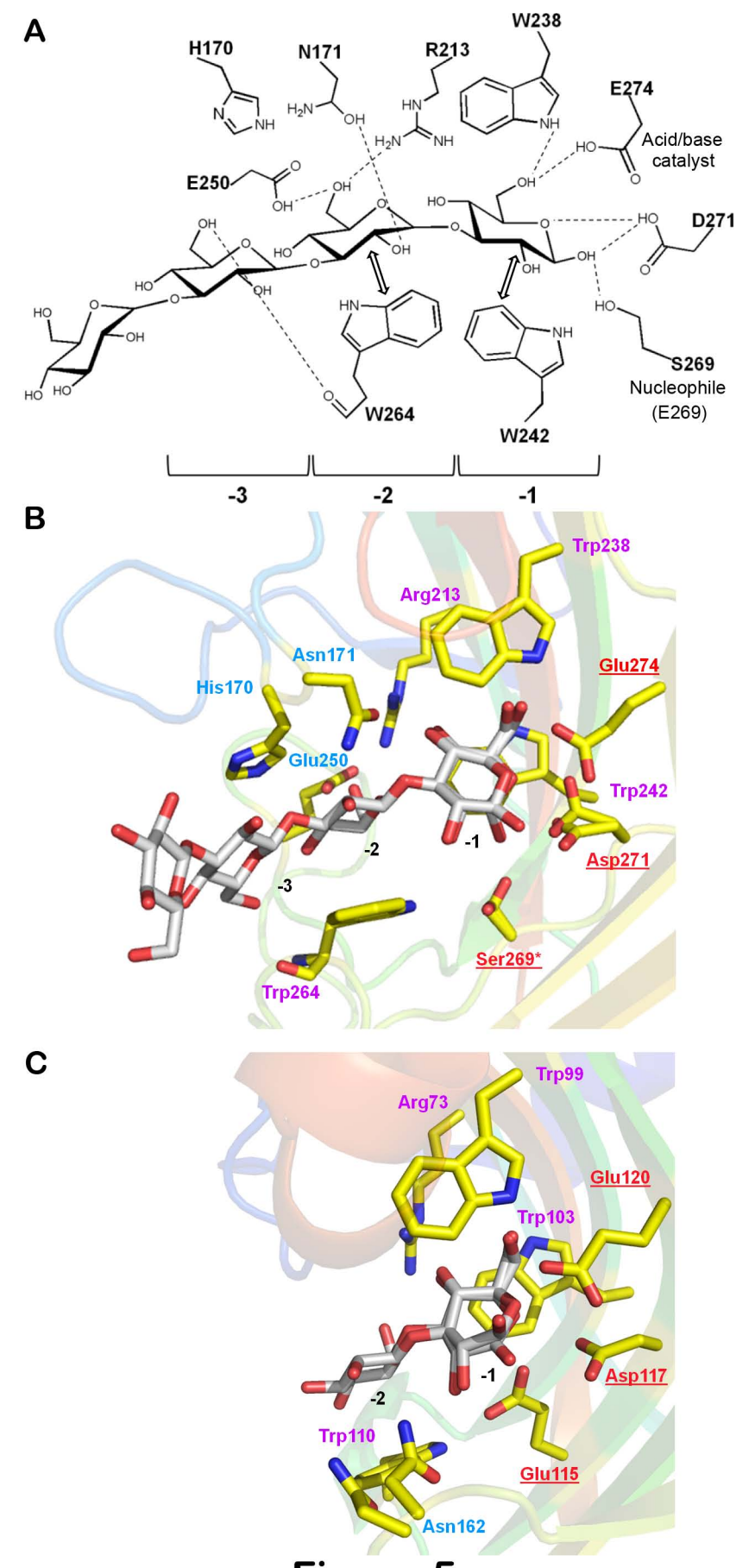
A
H170
N171
R213
W238
E274
Acid/base
catalyst
E250
D271
S269
Nucleophile
(E269)
W264
W242
-3
-2
-1
B
Trp238
Arg213
Asn171
His170
Glu274
Glu250
Trp242
-2
-1
-3
Asp271
Ser269*
Trp264
C
Trp99
Arg73
Glu120
Trp103
-1
-2
Asp117
Trp110
Glu115
Asn162

Figure 5

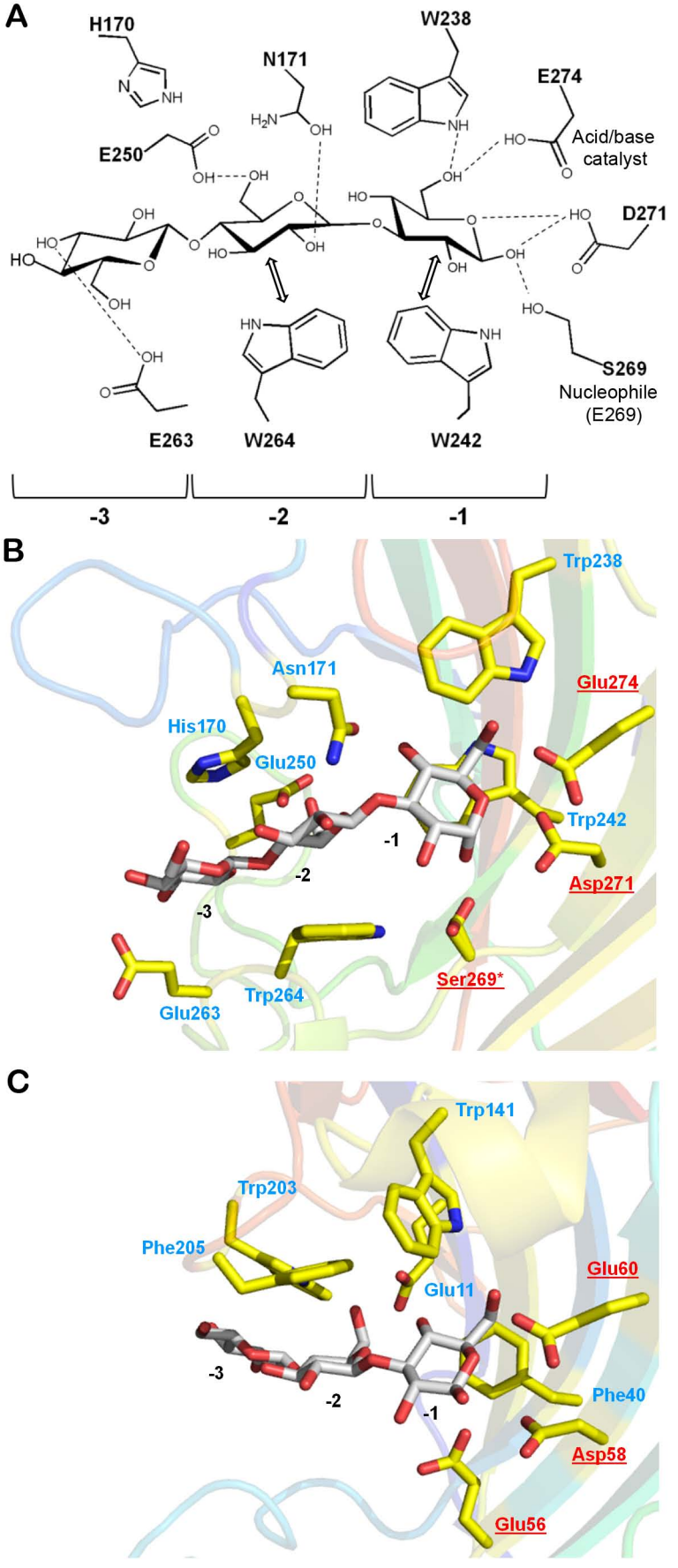
A
H170
N171
W238
E274
Acid/base catalyst
E250
D271
S269
Nucleophile (E269)
E263
W264
W242
-3
-2
-1
B
Trp238
Asn171
Glu274
His170
Glu250
Trp242
-1
-2
Asp271
-3
Ser269*
Trp264
Glu263
C
Trp141
Trp203
Phe205
Glu60
Glu11
-3
-2
-1
Phe40
Asp58
Glu56

Figure 6

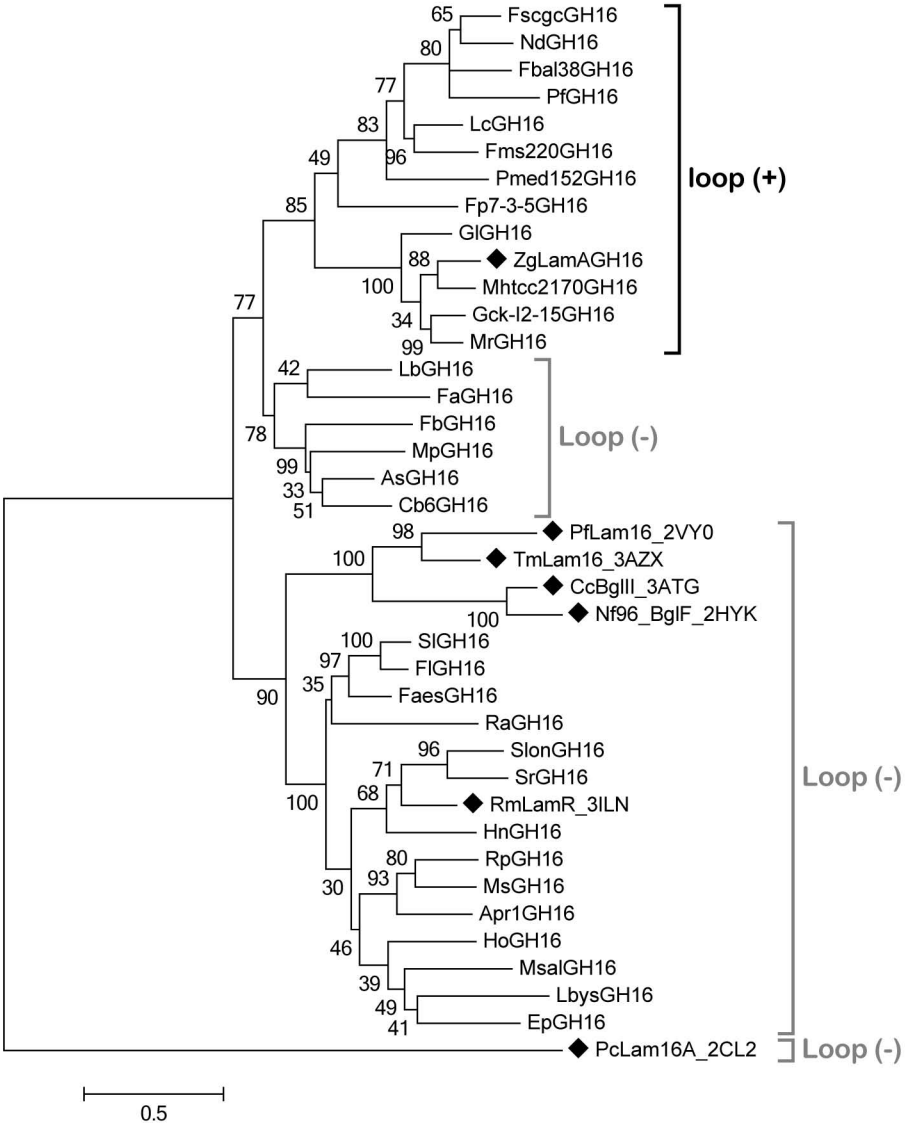
FscgcGH16
NdGH16
Fbal38GH16
PfGH16
LcGH16
Fms220GH16
Pmed152GH16
Fp7-3-5GH16
GlGH16
ZgLamAGH16
Mhtcc2170GH16
Gck-I2-15GH16
MrGH16
loop (+)
LbGH16
FaGH16
FbGH16
MpGH16
AsGH16
Cb6GH16
Loop (-)
PfLam16_2VY0
TmLam16_3AZX
CcBglII_3ATG
Nf96_BglF_2HYK
SlGH16
FlGH16
FaesGH16
RaGH16
SlonGH16
SrGH16
RmLamR_3ILN
HnGH16
RpGH16
MsGH16
Apr1GH16
HoGH16
MsalGH16
LbysGH16
EpGH16
Loop (-)
PcLam16A_2CL2
Loop (-)
0.5

Figure 7